Article

Heme-FeIII Superoxide, Peroxide and Hydroperoxide Thermodynamic Relationships: FeIII-O2•– Complex H-Atom Abstraction Reactivity

Hyun Kim, Patrick J. Rogler, Savita K Sharma, Andrew W. Schaefer, Edward I. Solomon, and Kenneth D. Karlin

J. Am. Chem. Soc., **Just Accepted Manuscript** • DOI: 10.1021/jacs.9b12571 • Publication Date (Web): 08 Jan 2020

Heme-Fe^{III} Superoxide, Peroxide and Hydroperoxide Thermodynamic Relationships: Fe^{III}-$O_2^{\bullet-}$ Complex H-Atom Abstraction Reactivity

Hyun Kim,† Patrick J. Rogler,† Savita K. Sharma,† Andrew W. Schaefer,‡ Edward I. Solomon,*,‡ and Kenneth D. Karlin*,†

†Department of Chemistry, Johns Hopkins University, Baltimore, Maryland 21218, United States
‡Department of Chemistry, Stanford University, Stanford, California 94305, United States

ABSTRACT: Establishing redox and thermodynamic relationships between metal ion bound O_2 and its reduced (and protonated) derivatives is critically important for a full understanding of (bio)chemical processes involving dioxygen processing. Here, a ferric heme peroxide complex, $[(F_8)Fe^{III}\text{-}(O_2^{2-})]^-$ (***P***) (F_8 = tetrakis(2,6-difluorophenyl)porphyrinate), and superoxide complex, $[(F_8)Fe^{III}\text{-}(O_2^{\bullet-})]$ (***S***), are shown to be redox interconvertible. Using $Cr(\eta\text{-}C_6H_6)_2$, an equilibrium state where ***S*** and ***P*** are present was established in tetrahydrofuran (THF) at –80 °C, allowing reduction potential determination of ***S*** as –1.17 V vs. $Fc^{+/0}$. ***P*** could be protonated with 2,6-lutidinium triflate, yielding the low-spin ferric hydroperoxide species, $[(F_8)Fe^{III}\text{-}(OOH)]$ (***HP***). Partial conversion of ***HP*** back to ***P*** using a derivatized phosphazene base gave a ***P***/***HP*** equilibrium mixture; leading to the determination, pK_a = 28.8 for ***HP*** (THF, –80 °C). With the measured reduction potential and pK_a, the O–H bond dissociation free energy (BDFE) of hydroperoxide species ***HP*** was calculated to be 73.5 kcal/mol, employing the thermodynamic square scheme and Bordwell relationship. This calculated O–H BDFE of ***HP*** in fact lines up with an experimental demonstration of the oxidizing ability of ***S***, via hydrogen atom transfer (HAT) from TEMPO–H (2,2,6,6-tetramethylpiperdine-N-hydroxide, BDFE = 66.5 kcal/mol in THF), forming the hydroperoxide species ***HP*** and TEMPO radical. Kinetic studies carried out with TEMPO–H(D) reveal second-order behavior, k_H = 0.5, k_D = 0.08 $M^{-1}s^{-1}$ (THF, –80 °C), thus the hydrogen/deuterium kinetic isotope effect (KIE) = 6, consistent with H-atom abstraction by ***S*** to be the rate-determining step. This appears to be the first case where experimentally derived thermodynamics lead to a ferric heme hydroperoxide OO–H BDFE determination, that Fe^{III}-OOH species being formed via HAT reactivity of the partner ferric heme superoxide complex.

INTRODUCTION

Cytochrome P450 monooxygenases (CYP450s) catalyze the incorporation of one atom of molecular oxygen into biological substrates, i.e., they hydroxylate nonactivated C–H bonds in hydrocarbon and various other compounds.[1–10] CYP450s are involved in critical biological processes, including the biosynthesis of steroid hormones, degradation of pharmaceutically derived drugs and detoxification of xenobiotics including carcinogens.[11–14] Many excellent review articles concerning CYP450s exist, covering the relevant biochemistry, summarizing available protein X-ray structures[15,16] and detailing aspects of the nature of intermediates and reaction mechanism. Theoretical/computational investigations and analyses have been part of the research efforts.[1,3,5,10,17–21]

The CYP450 catalytic mechanism as currently accepted is depicted in Scheme 1. When the substrate (R–H) approaches the heme active-site, it displaces the distally bound axial water molecule from the six-coordinate low-spin ferric ion, converting it to a five-coordinate, high-spin ferric-porphyrinate. The loss of the H_2O causes an increase of the redox potential of the heme iron by approximately 300 mV,[4] which enables electrons transfer from the biological reductase producing a five-coordinate ferrous porphyrinate. Note that in the resting state, the Fe^{III}/Fe^{II} reduction potential ranges between –400 and –170 mV, and thus is inactive to reduction.[2] The ferrous heme binds dioxygen, giving rise to the initial ferric superoxide intermediate, often referred to as the oxy-heme or oxy ferrous intermediate. The addition of a second electron converts superoxide to a ferric peroxide intermediate, and this step is overall rate-determining in the CYP450 catalytic cycle.[17,22] Subsequently, the peroxide is protonated to form a low-spin ferric hydroperoxide intermediate, Fe^{III}–OOH, which is known as Compound 0. A second protonation on the distal oxygen of hydroperoxide species causes heterolytic O–O bond cleavage to produce a highly reactive high-valent ferryl–oxo π-cation porphyrinate radical (Cmpd I), releasing a molecule of water. Cmpd I is accepted as the active substrate oxidant for the normal CYP450 cycle.[9,23] This species abstracts a hydrogen atom from the substrate to give a radical (R•) and the "OH" from the resulting iron(IV)-OH (Cmpd II) undergoes 'rebound'[24] to the substrate radical, giving products R–OH plus the original (in the cycle) ferric heme.

Scheme 1. Catalytic Cycle of Cytochrome P450 Monooxygenases (where R–H is the substrate).[8]

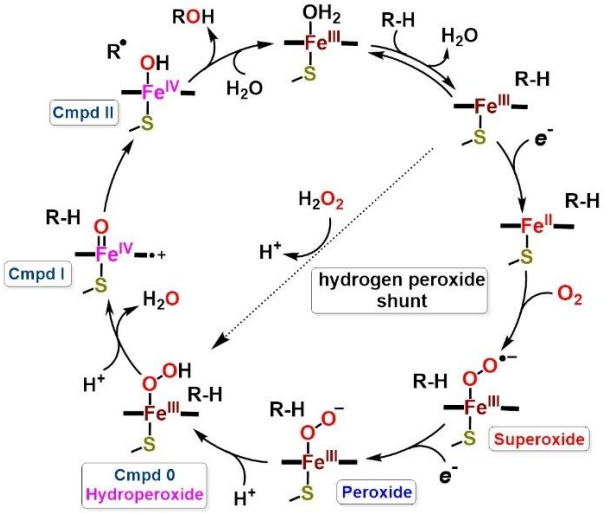

As shown in Scheme 1, superoxide/peroxide/hydroperoxide intermediates are involved in catalytic cycle of CYP450. These species also have been observed as intermediates in biological processes involving other O_2 or H_2O_2 activating heme enzymes.[6] These include heme oxygenase (HO; oxidatively breaking down hemes while also effecting release of iron and CO (or other metabolite): superoxide (Fe^{II}-O_2) and hydroperoxide),[25–27] nitric oxide synthase (NOS; two-step reaction where hydroxylation of L-arginine to N-hydroxy-L-arginine (L-NHA) is followed by oxidation of L-NHA to citrulline and $NO_{(g)}$: superoxide, peroxide, and hydroperoxide),[28,29] steroid hormone multifunctional CYPs (hydroxylation and lyase activities: superoxide, peroxide, and hydroperoxide),[30–32] horseradish peroxidase (HRP; H_2O_2 mediated substrate oxidation: hydroperoxide),[6,9,33,34] chloroperoxidase (CPO; H_2O_2 mediated substrate halogenation: hydroperoxide),[9,35] aromatic peroxygenase (APO; oxygenation of aliphatic and aromatic hydrocarbons: hydroperoxide),[9,36] and tryptophan 2,3-dioxygenase (TDO; transformation to formylkynurenine: superoxide).[6,37] Any and all aspects of CYP or other O_2/H_2O_2 activating heme enzymes (vide supra) reaction mechanisms have been or are being investigated, including what key protonation events take place and how, and what the structures of all intermediates are such as atom-connectivity along with bonding (electronic structure). The initial oxy-heme, the O_2-adduct with ferrous ion (i.e., the ferric superoxide),[38] the subsequently reduced intermediate peroxide and protonated hydroperoxide (Cmpd 0) have not been detected in normal enzyme turnover. However, comprehensive radiolytic cryoreduction studies[25,39–42] have provided many details concerning their structures and physical properties. Theoretical/computational investigations have also provided insights into the structures and thermodynamic inter-relationships for intermediates in the CYP450 catalytic cycle (Scheme 1).[5]

However, over the years and continuing on, generation of synthetic analogs of all the intermediates relevant to the CYP450 catalytic cycle has been of great interest (and importance). In this regard, there are many known heme Fe^{III}-superoxide synthetic compounds,[8,43–52] O_2-adducts of reduced ferrous hemes, including hemoglobin/myoglobin mimics such as the "Picket-Fence" porphyrin O_2-adduct.[43] However, these do not possess thiolate axial ligation as in CYP450s. Ferric heme peroxide and ferric heme hydroperoxide complexes are relatively rare (and see discussions below) even though researchers have suggested that hydroperoxide species may serve as alternative oxidant, since it is a common intermediate in the catalytic cycles of monooxygenases.[19,53–55]

Reviews emphasizing synthesis and reactivity of M^{n+}-($O_2^{\bullet-}$) complexes are now available.[56,57] Many M^{n+}-($O_2^{\bullet-}$) complexes of the first row transition metals, for example Mn, Fe, Co, Ni, Cu and Zn have been synthesized via metal-complex + O_2 or metal-complex + superoxide reactions and their substrate reactivity investigated. Iron-superoxide species are considered to form in the first step of dioxygen activation as the reactive intermediates in heme (vide supra) and non-heme metalloenzymes (e.g., Myo-inositol oxygenase (MIOX) and isopenicillin-N-synthase (IPNS)).[57]

In this report, we describe new synthetic analogues of those intermediates early in the cycle, prior to O–O cleavage, namely the ferric heme superoxide, peroxide and hydroperoxide species (***S***, ***P*** and ***HP***, respectively (Figure 1)). We note that in CYP450, the superoxide, peroxide and hydroperoxide intermediates are thought to have an end-on structure,[9,10,58] only binding to iron with one oxygen atom (the proximal O-atom), as depicted in Scheme 1. Utilizing the F_8 (F_8 = tetrakis(2,6-difluorophenyl)porphyrinate) heme framework, we have spectroscopically characterized corresponding ***S***, ***P*** and ***HP*** complexes, with UV-vis, electron paramagnetic resonance (EPR) and resonance Raman (rR) spectroscopies, and further chemically confirmed that ***P*** and ***HP*** are peroxidic (vide infra).

More importantly, and the primary advance described in this report, is that we have experimentally established the thermodynamic relationships between these complexes: (1) The reduction of ferric superoxide compound ***S*** is reversible, using chemical reagents, and a reduction potential $E°'$ has been determined, (2) the ferric peroxo complex ***P***, possessing an intermediate spin and side-on bound peroxide dianion ligand, can be reversibly protonated to give the low-spin ferric hydroperoxide ***HP***. Thus, a pK_a value for ***HP*** has been established. Further, another finding is that the ferric heme superoxide complex ***S*** can effect a hydrogen atom abstraction reaction, and directly produce ferric heme hydroperoxide complex ***HP*** (Figure 1). Only recently, Dey and co-workers[44] demonstrated for the first time that a ferric heme superoxide complex could effect a HAT reaction; removal of a hydrogen atom from a porphyrinate appended catechol, thus an intra-molecular process, converted the superoxide complex to the hydroperoxide analog. Such a transformation represents the diagonal part of a thermodynamic square scheme, relating ***S***, ***P*** and ***HP*** complexes (Figure 1). Now, with our measured reduction potential ($E°'$) and pK_a values (as mentioned above), the O–H bond dissociation free energy (BDFE) of ferric heme hydroperoxide complex ***HP*** could be determined using the Bordwell relationship (eq. 1) where $C_{G,solv}$ represents the $H^+/H^\bullet$ standard reduction potential in a particular solvent (also see below).[59]

$$BDFE = 1.37(pK_a) + 23.06E^o + C_{G,solv} \quad (1)$$

Further, the calculated BDFE of complex ***HP***, in fact is shown to be in-line (consistent) with the actual experimental reactivity of ***S*** toward a substrate with O–H bond (vide infra). To

the best of our knowledge, the present study reports the first example showing thermodynamics (reduction potential and pK_a) involved and the generation of the ferric heme hydroperoxide species by ferric heme superoxide complex via HAT of an exogenously added substrate.

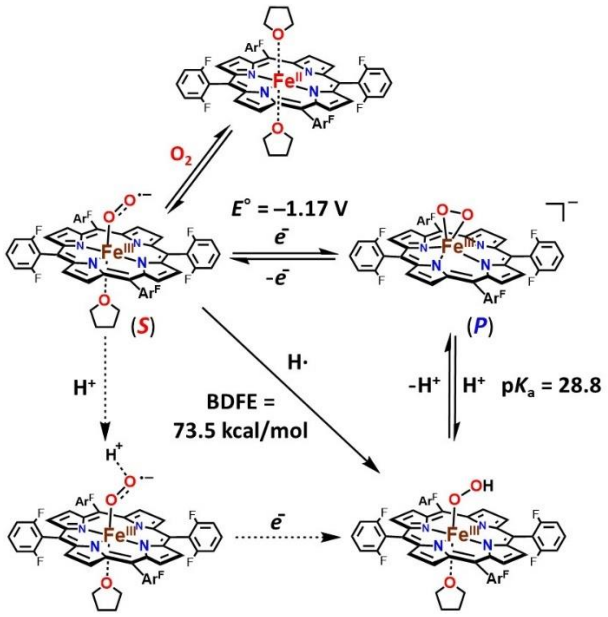

Figure 1. Sequential preparation of superoxide/peroxide/hydroperoxide heme analogs and thermodynamic square scheme of reduction ($E°$ as determined vs $Fc^{+/0}$) and protonation of a F_8 ferric heme superoxide analog and O–H BDFE of ferric heme hydroperoxide. (Ar^F = 2,6-difluorophenyl group)

RESULTS AND DISCUSSION

Generation and Characterization of a Side-on Heme Ferric Peroxide, [(F_8)Fe^{III}-(O_2^{2-})]$^-$ (*P*). As reported in previous work,[60] addition of the outer sphere strong reductant $CoCp_2$ to the previously well-characterized ferric superoxide complex [(F_8)Fe^{III}-($O_2^{\bullet-}$)] (*S*) (λ_{max} = 416 and 535 nm; rRaman, ν_{O-O}, 1178 cm^{-1} ($\Delta^{18}O_2$, –64 cm^{-1}); ν_{Fe-O}, 568 cm^{-1} ($\Delta^{18}O_2$, –24 cm^{-1}))[61,62] at –80 °C in THF yields side-on ferric heme-peroxide complex [(F_8)Fe^{III}-(O_2^{2-})]$^-$ (*P*) with UV-vis spectral features at 434, 541 and 561 nm (Figure 2A). These electronic absorption spectra are the same as those known for other previously well-characterized side-on ferric porphyrin peroxide complexes which have low energy Soret band and two peaks between 500 and 600 nm at α, β-region.[11,48,63,64] Valentine and co-workers[63] originally discovered and characterized such species and synthesized them by the reaction of potassium superoxide solubilized with 18-crown-6 ether, where the first superoxide anion reduced a porphyrinate-Fe^{III}Cl (porphyrinate-H_2 = TPP, OEP)[65] to the Fe^{II} form which then reacted with another equiv of superoxide anion to give the [(porphyrinate)Fe^{III}(O_2^{2-})]$^-$ species with side-on bound peroxide ligand (see diagram below). These species do not possess an additional axial ligand, as deduced previously,[11,48,63,64] and supported by the X-ray structure of a manganese analog [(TPP)Mn(η^2-O_2^{2-})]$^-$; here the Mn^{III} ion lies well above the porphyrinate plane toward the peroxo ligand.[66,67]

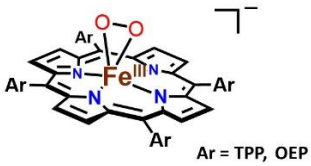

Previously, our complex ***P*** was characterized by UV-vis, EPR (g = 4.2 (S = 3/2); see Figure S1) and ^{1}H NMR spectroscopies.[60] Further characterization of ***P*** was carried out and ^{2}H NMR and rR spectroscopies are presented here. The pyrrolic proton in ^{2}H NMR spectroscopy at –80 °C resonates at δ 92.7 ppm (Figure S2), and this feature is consistent with the previously reported ^{1}H NMR spectroscopic signature (90 ppm).[60] Resonance Raman experiments confirmed peroxide formulation for ***P***, with the observation of ν_{O-O} vibration (806 cm^{-1}, $\Delta^{18}O_2$ = –46 cm^{-1}) and ν_{Fe-O} stretch (466 cm^{-1}, $\Delta^{18}O_2$ = –19 cm^{-1}) as shown in Figure 2B. These observed stretching frequency values match those calculated using the harmonic oscillator model: $\Delta_{O-O,calc}$ ($^{16}O_2/^{18}O_2$) = –47 cm^{-1}, $\Delta_{Fe-O,calc}$ ($^{16}O_2/^{18}O_2$) = –21 cm^{-1}. The relatively low Fe–O stretching frequency, which results from the symmetric stretching vibration of a side-on bound peroxide ligand, is similar to that in two other similarly structured heme peroxo compounds (vide infra, Table S1)[48] as well as non-heme[68–70] side-on peroxide complexes. It is notable that ν_{Fe-O} in these compounds is considerably reduced compared to what is observed for oxy-heme (i.e., Fe^{II}-(O_2)) species like oxy-myoglobin (ν_{Fe-O} = 570 cm^{-1}),[71] which we are referring to as ferric superoxide complexes. When strong acid, triflic acid (HOTf), is utilized to protonate peroxide species ***P***, H_2O_2 is released as expected and a yield of 95.5% is obtained (see Experimental Section and Figure S3). If no hydrogen peroxide had been released with the acidification, it would have likely meant that reductive O–O cleavage (to give water) had somehow occurred.[72,73]

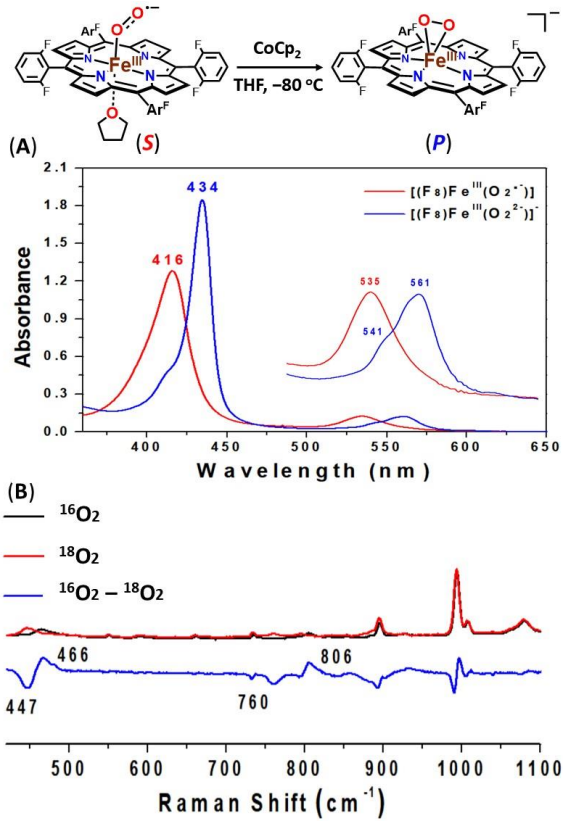

Figure 2. (A) UV-vis spectra of [(F$_8$)Fe^{III}-(O$_2$•$^-$)] (***S***) (red) to [(F$_8$)Fe^{III}-(O$_2^{2-}$)]$^-$ (***P***) (blue) in THF at –80 °C. (B) Resonance Raman spectra of ferric peroxide complex ***P*** in frozen THF obtained at 77 K with 413 nm excitation: Fe–O and O–O stretching frequencies for the complex generated with $^{16}O_2$ (black) or $^{18}O_2$ (red). The $^{16}O_2$–$^{18}O_2$ difference spectrum is shown in blue. The bands at 900 and 1000 cm^{-1} are vibrations within the porphyrin ring, which are generally observed for hemes and minimally impacted by O_2 isotope substitution (i.e. the modes contain minimal O_2 motion). For full spectrum of ***P***, see Figure S4.

Generation and Characterization of an End-on Hydroperoxide Species, [(F$_8$)Fe^{III}-(OOH)] (*HP*). The addition of one equiv 2,6-lutidinium triflate [(LutH$^+$)](OTf) or [(H)DMF](OTf)[74] to the solution of [(F$_8$)Fe^{III}-(O$_2^{2-}$)]$^-$ (***P***) at –80 °C in THF leads to protonation of this side-on ferric heme peroxide complex to form a corresponding ferric heme hydroperoxide species, [(F$_8$)Fe^{III}-(OOH)] (***HP***). UV-vis spectra of ***HP*** exhibit absorptions at 418, 536 and 558 nm (Figure 3), while an EPR spectrum indicates distinctive changes from the side-on peroxide g = 4.2 signal observed in ***P***, to a low-spin ferric hydroperoxide species characterized by g = 2.23, 2.14 and 1.96 signals (Figure 4A), very similar to published values for other ferric end-on hydroperoxide synthetically derived complexes,[44,48,49,51,75–77] as well as for ferric heme hydroperoxides generated within hemoglobin and myoglobin.[78,79] Note that the full EPR spectrum (Figure S5) reveals that there is a small feature corresponding to leftover side-on ferric peroxide starting complex (at g = 4.2). Consistent with our complex formulation as [(F$_8$)Fe^{III}-(OOH)] (***HP***), a high yield (93.3%) of H_2O_2 was detected when we acidified the complex solution with triflic acid (HOTf) and applied the a quantitative horseradish peroxidase assay (see experimental section and Figure S3).[72,73]

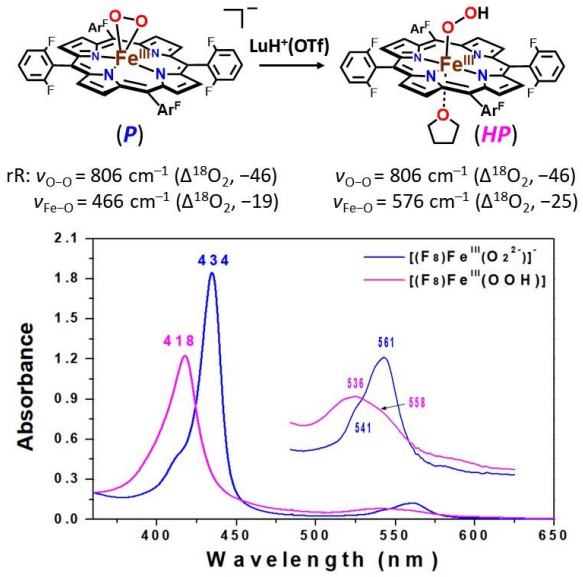

Figure 3. UV-vis spectra of illustrating the conversion of [(F$_8$)Fe^{III}-(O$_2^{2-}$)]$^-$ (***P***) (blue) to form [(F$_8$)Fe^{III}-(OOH)] (***HP***) (pink) by addition of [(LutH$^+$)](OTf) in THF at –80 °C.

The characterization of [(F$_8$)Fe^{III}-(OOH)] (***HP***) was further corroborated by rR spectroscopy. The rR spectra of ***HP*** are indicative of a clear change in the ν_{Fe-O} vibrational stretch mode on protonation, shifting from 466 cm^{-1} ($\Delta^{18}O_2$ = –19 cm^{-1}) in side-on ferric peroxide species ***P*** to 576 cm^{-1} ($\Delta^{18}O_2$ = –25 cm^{-1}) in hydroperoxide complex ***HP***, whereas the ν_{O-O} vibrational frequency remains the same, appearing at 806 cm^{-1} ($\Delta^{18}O_2$ = –46 cm^{-1}) as shown in Figure 4B. These ν_{Fe-O} and ν_{O-O} vibrational stretching frequency downshifts when using $^{18}O_2$ match well with values calculated using the harmonic oscillator model: $\Delta_{Fe-O,calc}$ ($^{16}O_2/^{18}O_2$) = –26 cm^{-1}, $\Delta_{O-O,calc}$ ($^{16}O_2/^{18}O_2$) = –47 cm^{-1}. Also, these observed ν_{Fe-O} and ν_{O-O} vibrational values are quite similar to those obtained in other low-spin end-on ferric heme hydroperoxide model complexes (Table S1), those from the groups of Naruta[48,49,51] and Dey[80] and their co-workers. This also well matches data obtained from cryogenically ferric hydroperoxide species generated in CYP450's,[81,82] even though the latter have axial cysteinate ligands which makes the coordination environment very different as compared to those for the synthetic analogues (Table S1). The combined spectroscopic data (UV-vis, EPR and rRaman) support the formulation of ***HP*** as a low-spin end-on (η^1) ferric hydroperoxide species. We postulate that ***HP*** most likely possesses a solvent THF molecule (Figure 3), as we know this can confer low-spin character to six-coordinate ferric hemes with F$_8$;[61,62,83] there exists the possibility the axial ligand is 2,6-lutidine or DMF, in exchange with THF.

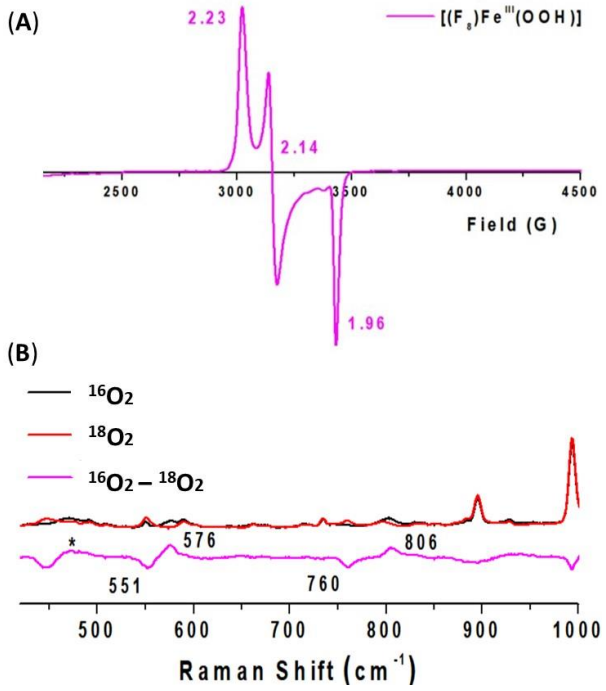

Figure 4. (A) Frozen THF solution EPR (10K) spectrum of ***HP***. For full spectrum of ***HP***, see Figure S5. (B) Resonance Raman spectra of ferric hydroperoxide complex ***HP*** in frozen THF obtained at 77 K with 413 nm excitation: Fe–O and O–O stretching frequencies for the complex generated with $^{16}O_2$ (black) or $^{18}O_2$ (red). The $^{16}O_2$–$^{18}O_2$ difference spectrum is shown in pink. Note that complex ***P*** is present as an impurity, observed as a set of $^{16}O_2$/$^{18}O_2$ peaks at 466/447 cm^{-1} (marked with an asterisk). For full spectrum of ***HP***, see Figure S4.

Comparison of This Work with Previously Reported Hydroperoxide Ferric Hemes. It has been generally difficult to cleanly synthesize ferric heme hydroperoxide compounds. Tajima and co-workers[75,77,84] reported low-spin ferric hydroperoxide complexes which are in accord with a Fe^{III}-heme(-OH)(-OOH) formulation, based on UV-vis and EPR spectroscopies. Significant advances were made by Naruta and co-workers[48] who extensively characterized an end-on ferric hydroperoxide complex, that shown in Figure 5B.[14,20] It was generated by protonation of the seven-coordinated side-on peroxide species [(TMPIm)Fe^{III}-(O_2^{2-})] (Figure 5A) with ligated axial imidazole ligand from the covalently attached tether, wherein a spin state change from S = 3/2 (ν_{Fe-O} = 470 cm^{-1} ($\Delta^{18}O_2$ = –19 cm^{-1}); ν_{O-O} = 809 cm^{-1} ($\Delta^{18}O_2$ = –45 cm^{-1})) to low-spin (ν_{Fe-O} = 570 cm^{-1} ($\Delta^{18}O_2$ = –26 cm^{-1}); ν_{O-O} = 810 cm^{-1} ($\Delta^{18}O_2$ = –47 cm^{-1})) occurred (Table S1).[48] Therein, a covalently appended axial imidazole ligand was critical to give a stable 6-coordinate ferric heme hydroperoxide complex. In the absence of the imidazolyl axial ligand (Figure 5), only decomposition occurred upon protonation. In other case, Anxolabéhère-Mallart and co-workers[76] generated a ferric heme hydroperoxide complex in the presence of 1-methylimidazole as sixth ligand by protonation of its side-on ferric peroxide precursor which is formed from the electrochemical reduction of an in situ formed ferric superoxide species. A significant difference in synthetic protocols occurs with our case (vide supra); while Naruta and co-workers postulated that methanol was the proton source converting peroxide to hydroperoxide complex, a stronger acid ([(LutH$^+$)](OTf) or [(H)DMF](OTf)) was required in our case, but a strong axial base ligand was not necessary.

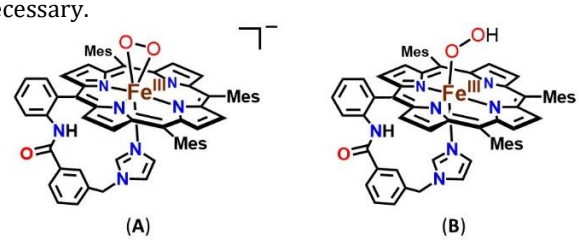

Figure 5. Naruta group's synthetic complexes; (A) [(TMPIm)Fe^{III}–(O_2^{2-})], (B) [(TMPIm)Fe^{III}–(OOH)].[48]

Reduction Potential of the [(F_8)Fe^{III}-($O_2^{\bullet-}$)] (*S*)/ [(F_8)Fe^{III}-(O_2^{2-})]$^-$ (*P*) Redox Couple. When we set out this study, one of the main goals was to see if we could determine a reduction potential for a superoxide [(F_8)Fe^{III}-($O_2^{\bullet-}$)] (***S***) conversion to side-on peroxide complex [(F_8)Fe^{III}-(O_2^{2-})]$^-$ (***P***). In order to do this accurately it needed to be shown that reduction of ***S*** to ***P*** is a reversible reaction. In fact, we find this to be the case; [(F_8)Fe^{III}-($O_2^{\bullet-}$)] (***S***) and peroxide [(F_8)Fe^{III}-(O_2^{2-})]$^-$ (***P***) are interconvertible using redox reagents. Addition of the strong oxidant, [(4-BrC_6H_4)$_3$N](SbCl_6) (Tris(4-bromophenyl)ammoniumyl cation, known as Magic Blue because of its intense royal blue color; $E_{1/2}$ = 0.67 V vs. $Fc^{+/0}$ in MeCN)[85] to the solution of ***P*** results in complete oxidative conversion of the peroxide to superoxide species (Figure 6).

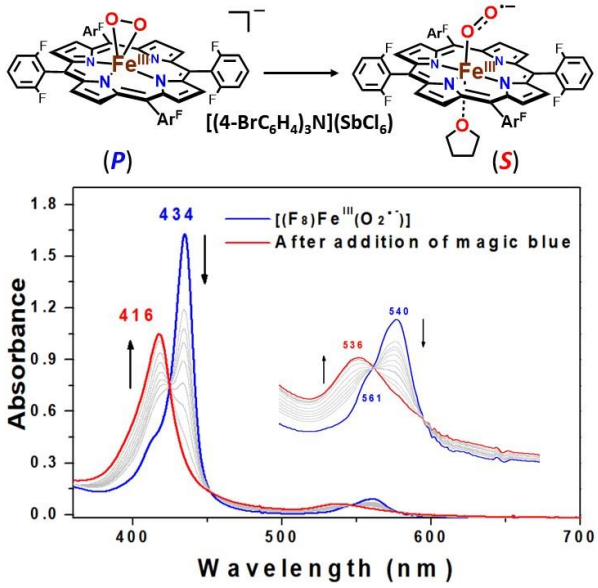

Figure 6. UV-vis spectra demonstrating the oxidation of [(F_8)Fe^{III}-(O_2^{2-})]$^-$ (***P***) (blue) to form [(F_8)Fe^{III}-($O_2^{\bullet-}$)] (***S***) (red) in THF at –80 °C. A spectrum (gray lines) was recorded every ~2 min; the reaction goes to completion in ~ 20 min. Also, see the text.

Observations supporting this conclusion are that the product solution containing [(F_8)Fe^{III}-($O_2^{\bullet-}$)] (***S***) is EPR silent (10 K, THF) as expected; the low-spin Fe^{III} ion is antiferromagnetically coupled with the unpaired electron of the

directly coordinated superoxide radical anion. Interestingly, the addition of the weaker reductant, Cr(η-C_6H_6)$_2$ ($E_{1/2}$ = –1.15 V vs. $Fc^{+/0}$ in CH_2Cl_2),[85] to the solution of ***S*** leads to the formation of an equilibrium mixture of superoxide ***S*** and peroxide ***P***, allowing the determination of the reduction potential for the superoxide (***S***)/peroxide (***P***) couple. A titration of superoxide ***S*** with varying amounts of Cr(η-C_6H_6)$_2$ in THF at –80 °C was monitored by UV-vis spectroscopy (Figure 7), allowing the determination of an equilibrium constant value in each instance of added bis-benzene chromium(0) titrant (Table S2); the UV-vis absorptions for ***S*** and ***P*** gave direct determination of their concentrations, thus defining the amount/concentration of Cr(η-C_6H_6)$_2$ reacted and of [Cr(η-C_6H_6)$_2$]$^+$ formed. From the collection of calculated equilibrium constants, corresponding reduction potentials were determined by using the Nernst equation. Thus, the reduction potential ($E°'$) for [(F_8)Fe^{III}-($O_2^{•-}$)] (***S***)/[(F_8)Fe^{III}-(O_2^{2-})]$^-$ (***P***) couple was calculated to be –1.17 ± 0.01 V vs. $Fc^{+/0}$ (for which $E°'$ = –0.39 V vs. SHE in THF). See Table S2 for further details. A further demonstration of the reversibility of the reduction and oxidation of complex ***S***/***P*** was established; Peroxide species ***P*** generated by Cr(η-C_6H_6)$_2$ could be fully oxidized back to superoxide ***S*** using Magic Blue and again, this resulting solution could be reduced to peroxide ***P*** with 5 equiv Cr(η-C_6H_6)$_2$, to the extent of ~85% (Figure S6).

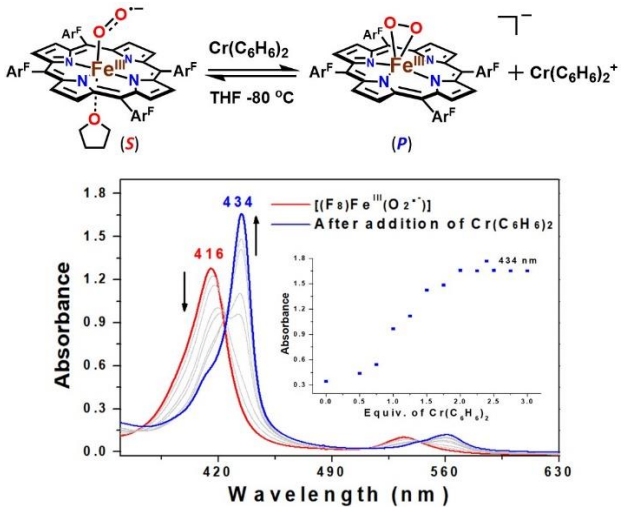

Figure 7. Conversion of [(F_8)Fe^{III}-($O_2^{•-}$)] (***S***) (red) to [(F_8)Fe^{III}-(O_2^{2-})]$^-$ (***P***) (blue) upon addition of Cr(η-C_6H_6)$_2$ in THF at –80 °C, resulting in the generation of equilibrium mixtures which allowed the determination of the reduction potential (–1.17 V vs. $Fc^{+/0}$) of the ***S***/***P*** redox couple. Inset: monitoring the absorbance at 434 nm upon addition of various amounts of Cr(η-C_6H_6)$_2$. See Table S2 for details.

Recently, Naruta and co-workers[51] reported the reduction potential (–0.67 V and –1.1 V vs. SHE) of various ferric heme superoxide synthetic compounds, not experimentally but by employing density functional theory (DFT) calculations. Thus, these values are much more negative than what was found by us for the [(F_8)Fe^{III}-($O_2^{•-}$)] (***S***)/[(F_8)Fe^{III}-(O_2^{2-})]$^-$ (***P***) redox couple, E°' = –0.39 V vs. SHE in THF at –80 °C. Anxolabéhère-Mallart, Fave and co-workers[76] recently reported on the electrochemical generation of the side-on peroxide species [Fe^{III}(F_{20}TPP)(O_2)]$^-$ (EPR; g = 4.2) by applying a cathodic potential (E_{app} = –0.60 V vs. SCE; –0.36 V vs. SHE) to the corresponding superoxide precursor in dimethylformamide at –30 °C. The electrochemical reduction was found to be irreversible, nevertheless the finding of ferric heme superoxide complex reduction at $E°'$ = –0.60 V vs. SCE (–0.36 V vs. SHE) is most interesting since it lies very close to our own result (vide supra). For Anxolabéhère-Mallart, Fave and co-workers, the superoxide and peroxide complexes employed the highly electron-withdrawing heme (F_{20}TPP) with 20 aryl fluorine substituents; no axial base ligand was utilized. Roughly, the comparison of reduction potential of –0.36 V for the F_{20}TPP containing ferric heme superoxide, as well as the –0.39 V value for reversible reduction of [(F_8)Fe^{III}-($O_2^{•-}$)] with the far more negative potentials (vide supra) observed for the various [(P)Fe^{III}-(O_2^{2-})] complexes from Naruta and co-workers, possessing a more electron-rich porphyrinate with axial imidazole ($TMPIm^{OH,OEt}$; Figure S7), may make sense. (See Table S3 for comparison of reduction potential values.)[86] Interestingly, computational chemists have estimated the reduction potential for the ferric heme superoxide species in CYP450 (Scheme 1); depending on "chosen model, QM region, and protonation state", the values obtained range from –2.28 to –1.04 V vs. SHE.[5] Perhaps this is most reasonable, as the axial cysteinate ligand in CYP450's is a strong anionic donor known for its ability to "push".[9,23]

Determination of the pK_a Value of [(F_8)Fe^{III}-(OOH)] (*HP*). As mentioned in the Introduction, for the thermodynamic square scheme, the pK_a value of hydroperoxide [(F_8)Fe^{III}-(OOH)] (***HP***) has been determined in THF at –80 °C. It was evaluated by spectral titration using the derivatized phosphazene base EtP_2(dma) (pK_a = 28.1 in THF, for the conjugate acid at room temperature, see diagram below).[87]

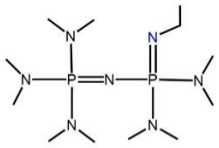

As shown by a titration followed by UV-vis spectroscopy (Figure 8), the absorption band at 418 nm of ***HP*** decreased with increasing concentration of added EtP_2(dma), and the absorption band shifted to 434 nm, with observation of an isosbestic point at 426 nm. Such additions gave rise to an equilibrium mixture of hydroperoxide ***HP*** and the side-on peroxide complex [(F_8)Fe^{III}-(O_2^{2-})]$^-$ (***P***) (see Table S4). From this data, an equilibrium constant for this reaction was calculated in each instance and using the known pK_a value of EtP_2(dma), a pK_a value for deprotonation of ***HP*** was determined to be 28.8 ± 0.5 (THF, –80 °C). Following addition of excess base EtP_2(dma), only the deprotonated complex ***P*** remained. As suggested by the data, the acid-base reaction interconversion of ***HP*** and ***P*** is reversible. This was further shown by adding [($LutH^+$)](OTf) to the solution generated in this titration (Figure 8), this gives the fully regenerated hydroperoxide complex ***HP*** (see Figure S8 for details). In order to corroborate the [(F_8)Fe^{III}-(OOH)] (***HP***) pK_a value

determined experimentally, a complementary experiment was conducted employing the conjugate acid of $EtP_2(dma)$, i.e., as expected, based on relative pK_a values, the addition of $EtP_2(dma)H^+$ (pK_a = 28.1) to peroxide $[(F_8)Fe^{III}\text{-}(O_2^{2-})]^-$ (***P***) results in the ready protonation and formation of ***HP*** (see Figure S9).

As discussed above, Naruta and co-workers[51] synthetically generated several ferric heme hydroperoxide complexes. They did address the question of pK_a values, but only computationally. For two ferric hydroperoxide complexes they described, possessing modified superstructured synthetic hemes (see Figure S7), their DFT determined pK_a values were 25.1 or 32.3 in EtCN as a solvent. In reality, these values are not so different from that of our own experimentally determined pK_a value (= 28.8, vide supra) for $[(F_8)Fe^{III}\text{-}(OOH)]$ (***HP***).

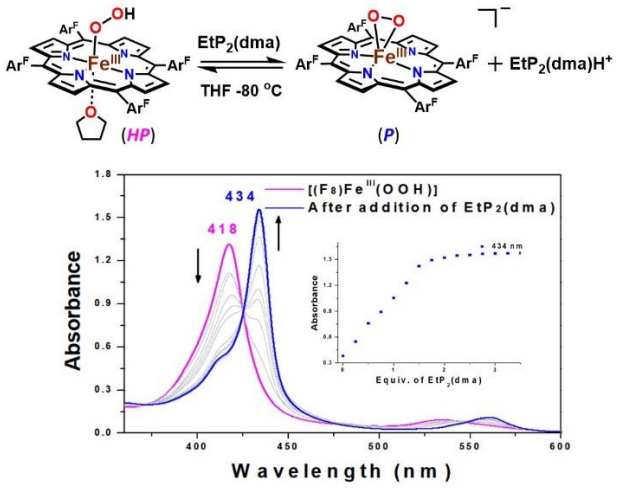

Figure 8. UV-vis spectroscopic monitoring of the incremental addition of $EtP_2(dma)$ to a solution of $[(F_8)Fe^{III}\text{-}(OOH)]$ (***HP***) (pink) resulting in the formation of equilibrium mixtures of ***HP***, $EtP_2(dma)$, $[(F_8)Fe^{III}\text{-}(O_2^{2-})]^-$ (***P***) (blue) and protonated base $EtP_2(dma)H^+$ which allowed the determination of the pK_a value (28.8) of ***HP***. Inset: monitoring of the absorbance at 434 nm (blue).

Determination of the OO–H BDFE of $[(F_8)Fe^{III}\text{-}(OOH)]$ (*HP*). The bond dissociation free energy (BDFE) is the thermodynamic parameter used to compare the energy, i.e., bond strength, for homolytic bond cleavage of a two atom-centered unit. In order to determine the BDFE, we utilized the Bordwell equation (eq. 1)[88] which uses Hess' law with the redox potential and acidity based on a thermodynamic cycle. Thus, using the measured thermodynamic parameters, $E°'$ (–1.17 V vs. $Fc^{+/0}$, vide supra) and pK_a (28.8, vide supra), a thermodynamic square scheme is completed as shown in Figure 1 and this leads to a BDFE of 73.5 ± 0.9 kcal/mol for the OO–H bond in hydroperoxide $[(F_8)Fe^{III}\text{-}(OOH)]$ (***HP***) according to eq. 2 where C_G is 61 kcal/mol in THF.[89]

$$\mathbf{BDFE}_{O\text{–}H} = 1.37(28.8) + 23.06(-1.17) + 61 = \mathbf{73.5\ kcal/mol} \quad (\mathbf{2})$$

As mentioned, this is to our knowledge the first case where a BDFE value has been reported using experimentally derived thermodynamics (reduction potential and pK_a) for a heme system, those involving O_2 or its reduced derivatives.[90] Morokuma and co-workers[91] computationally evaluated aspects of other heme-superoxide (as well as other metal-superoxide) species, and their findings are also in accord with the present results, i.e., that for $[(F_8)Fe^{III}\text{-}(OOH)]$, BDFE = 73.5 kcal/mol. For heme ferric superoxide complexes modeling protein active sites (e.g., hemoglobin, CYP450) where a proximal ligand is either an imidazole or an -SH group (the latter as a computational model for the cysteinate proximal ligand in CYP450's), i.e., (B)(porphyrinate)$Fe^{III}\text{-}O_2^{\bullet-}$ (B = imidazole, SH) the ferric heme hydroperoxide complex OO–H BDE's are calculated to be in the range 64–66 kcal/mol. Lai and Shaik[18] also computationally found that a CYP450 ferric heme superoxide is a "sluggish oxidant".

Corresponding OO–H BDFE (or BDE) values for a few product non-heme iron-hydroperoxide complexes are known, but these tetramethylcyclam (TMC) ligand derived complex results come only through computational evaluation.[91,92] These have recently been compared to experimental results on cobalt and other heavier metal-superoxide complexes.[93] Dicopper(II)-μ-hydroperoxide complex OO–H BDFE's have recently been determined.[89,94] In one case, the BDFE is 72 kcal/mol, while in another example, the binucleating ligand utilized results in a hydroperoxide OO–H BDFE of 81 kcal/mol. Thus, the corresponding dicopper(II)-μ-superoxide complex is a quite strong oxidant for HAT reactivity. Experimentation and compilation of O–H bond thermodynamic parameters (i.e., BDE's or BDFE's) of dioxygen-derived species (M-OH, M-OOH or M-oxo species formed from O_2-reduction/protonation) bound to metal complexes, is of considerable general significance and importance.[95]

Reactivity Studies of $[(F_8)Fe^{III}\text{-}(O_2^{\bullet-})]$ (*S*) with O–H, C–H and N–H substrates through HAT to Support for Our Calculated BDFE. One of the utilities of BDFE data is to determine or estimate the oxidative reactivity in this case of the ferric heme superoxide complex. Hydrogen atom transfer oxidation of substrates for $[(F_8)Fe^{III}\text{-}(O_2^{\bullet-})]$ (***S***) would afford the corresponding hydroperoxide analog, $[(F_8)Fe^{III}\text{-}(OOH)]$ (***HP***). With an ***HP*** BDFE experimentally determined to be 73.5 kcal/mol, we can expect that ***S*** would only be capable of HAT reactions with substrates such as C–H, N–H or O–H BDFE's below or near this value.[96] So, we have probed these possibilities. Addition of an excess of higher BDFE substrates than 73.5 kcal/mol (i.e., *p*-methoxyphenol, BDFE = 83.1 kcal/mol in THF; fluorene, 76.8 kcal/mol in THF; 9,10-dihydroanthracene, 76 kcal/mol in DMSO; *p*-OMe-2,6-di-tert-butylphenol, 75.8 kcal/mol in THF)[59,89] to solutions of $[(F_8)Fe^{III}\text{-}(O_2^{\bullet-})]$ (***S***) at –80 °C in THF led to no reaction, as expected. Also, no reaction occurs with similar BDFE substrates for ***HP***, such as 1,4-cyclohexadiene (72.9 kcal/mol in MeCN) and xanthene (72.2 kcal/mol in THF).[89] By contrast, BNAH (1-benzyl-1,4-dihydronicotinamide, 70.7 kcal/mol in DMSO),[97] phenylhydrazine (70.4 kcal/mol in MeCN) and diphenylhydrazine (67.1 kcal/mol in DMSO)[59] do react rapidly with complex ***S***, but we were not able to determine if the initial reaction is actually HAT; based on UV-vis spectroscopic monitoring, the expected hydroperoxide product,

[(F_8)Fe^{III}-(OOH)] (***HP***), was not observed at the end of the reaction; probably HAT occurs, but side-reactions prevent clean formation of ***HP***. However, the addition of TEMPO–H (66.5 kcal/mol in THF)[89] to a solution of ***S*** in THF at –80 °C led to shifting of the UV-vis spectrum (Figure 9A), i.e., yielding an absorption at 418 nm, corresponding to ***HP***, suggesting that substrate hydrogen atom abstraction reaction occurred. Note that this HAT reaction from TEMPO–H to complex ***S*** is thermodynamically downhill by ca. 7 kcal/mol, thus predicted to be quite favorable.

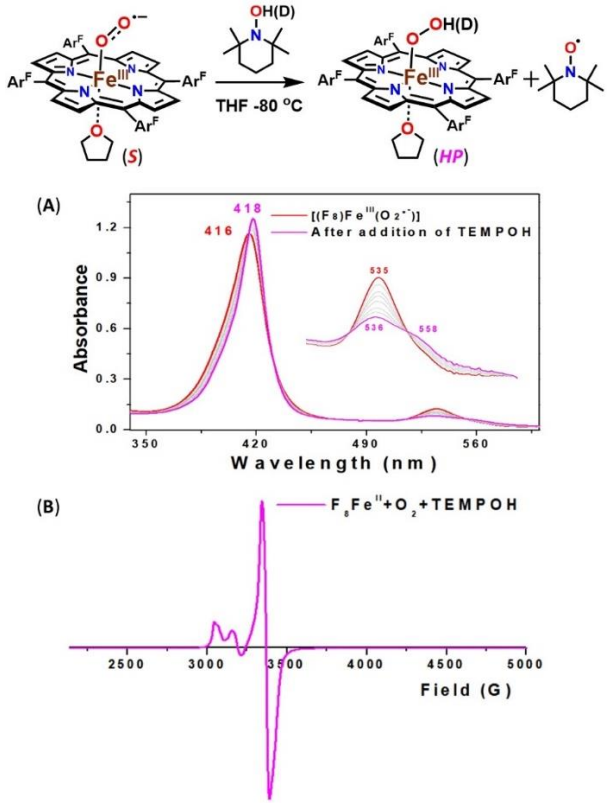

Figure 9. (A) UV-vis spectroscopic monitoring the reaction of [(F_8)Fe^{III}-($O_2^{\bullet-}$)] (***S***) (red) with TEMPO–H in THF at –80 °C to yield [(F_8)Fe^{III}-(OOH)] (***HP***) (pink). (B) 10 K EPR spectrum of the final products of TEMPO–H HAT by ***S*** in frozen THF. The yield of hydroperoxide ***HP*** is 94.2 % based on the absorbance and known absorptivity of ***HP*** at 418 nm. Spin quantification finds that the EPR signal corresponds to 92% of TEMPO radical.

Complementary experiments were performed, confirming generation of hydroperoxide species from the reaction between [(F_8)Fe^{III}-($O_2^{\bullet-}$)] (***S***) and TEMPO–H. For one thing, addition of EtP_2(dma) base to the product mixture led to the formation of peroxide species ***P*** based on UV-vis spectroscopy (Figure S10). Further, frozen solution EPR spectroscopy was also performed and this revealed a signal at g = 2 attributed to the TEMPO radical, appearing 'on top of' the signal expected for low-spin ***HP*** (Figure 9B), confirming H-atom abstraction by ***S*** from TEMPO–H. In addition, the final product exhibits upfield-shifted pyrrole resonance (δ_{pyrr} – 0.63 ppm) in ^{2}H NMR spectroscopy, indicative of a six-coordinate ferric low-spin (S = 1/2) heme (Figure S2).[98,99]

For further insights into the nature of the hydrogen atom abstraction from TEMPO–H by ***S***, kinetic studies were carried out in THF at –80 °C via UV-vis spectroscopy (Figure 9). The rate of formation of hydroperoxide ***HP*** obeyed pseudo-first-order kinetics (Figure S11) when the reaction was conducted with excess TEMPO–H, and the observed pseudo-first-order constants (k_{obs}) are proportional to concentrations of TEMPO–H as shown in Figure 10 with an effectively zero intercept within error. According to this plot of k_{obs} vs [TEMPO–H], the second order rate constant k_2 was obtained to be 0.5 $M^{-1}s^{-1}$ in THF at –80 °C. When deuterated substrate, TEMPO–D, was treated to [(F_8)Fe^{III}-($O_2^{\bullet-}$)] (***S***), a significant slowing of the reaction occurred; k_2 = 0.08 $M^{-1}s^{-1}$ in THF at –80 °C (Figure S12). The comparison of the rate constants for H vs. D provides for a significant kinetic deuterium isotope effect (KIE) of 6 in THF at –80 °C as shown in Figure 10, strongly suggesting that H-atom abstraction by ***S*** is the rate-determining step.

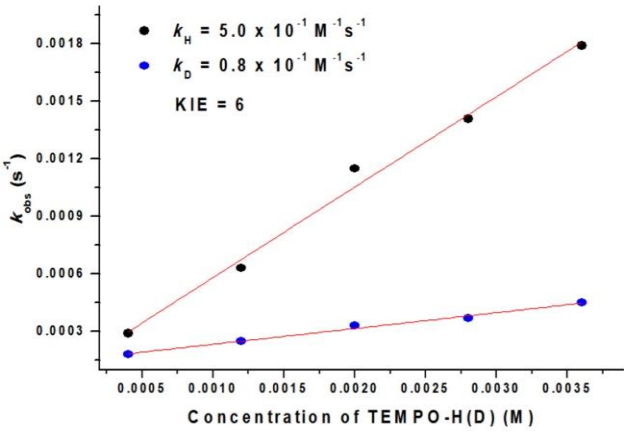

Figure 10. Plots of pseudo first order rate constants (k_{obs}) plotted against various concentrations of TEMPO–H(D) to obtain the second order rate constant, k_H = 5.0 x 10^{-1} $M^{-1}s^{-1}$ (black circle) and k_D = 0.8 x 10^{-1} $M^{-1}s^{-1}$ (blue circle) and KIE in THF at –80 °C.

There have been no prior reports of kinetic information to compare the reactivity of [(F_8)Fe^{III}-($O_2^{\bullet-}$)] (***S***) with other heme-superoxide complexes reacting with TEMPO–H. {Note: There is a study from Mayer and co-workers,[100] where a heme Fe^{III}-OH complex reacts with TEMPO–H, k_2 = 76 $M^{-1}s^{-1}$ at room temperature in toluene}. However, second order rate constants (k_2) for non-heme metal-superoxide (i.e., M^{n+}-($O_2^{\bullet-}$)) complexes (M = Cu, Mn, Co and Cr) involved in HAT reactions with TEMPO–H have been reported in a number of cases (see Table S5).[93,94,101–104]

As mentioned in the Introduction, recent review articles detail metal-superoxide complexes of the first row transition metals.[56,57] Prior computationally derived generalizations concerning metal superoxide reactivity have been published;[91,105] substrate reactivity depends on factors such as electrophilicity, reaction driving force, and coupling between the metal center and superoxide ligand. A CYP450 ferric superoxide is a weak oxidant for HAT, possessing large activation energy barriers.[18] These results are

consistent with our findings where superoxide complex reacts by HAT with an exogenous weak O–H (and perhaps N–H and C–H, vide supra) substrate. Also, a few potentially biologically relevant non-heme iron superoxide complexes are capable of abstracting hydrogen atom from weak X–H substrates such as 2,4-di-tert-butyl phenol,[106] 2-hydroxy-2-azaadamantane (AZADOL), phenylhydrazine (X–H < 72.6 kcal/mol)[107] and 9,10-dihydroanthracene (DHA; BDE = 76 kcal/mol).[108,109]

CONCLUSION

We report here that the side-on ferric peroxide species $[(F_8)Fe^{III}\text{-}(O_2^{2-})]^-$ (***P***) generated from $[(F_8)Fe^{III}\text{-}(O_2^{\bullet-})]$ (***S***) by one electron reduction, is protonated by acids such as $[(LutH^+)](OTf)$ to form the end-on ferric hydroperoxide complex $[(F_8)Fe^{III}\text{-}(OOH)]$ (***HP***) which has been characterized by UV-vis, EPR and rR spectroscopies. Thus, the stepwise generation of superoxide (***S***), peroxide (***P***) and hydroperoxide (***HP***) analogs which are involved in catalytic cycle of CYP450 (Scheme 1) or many other heme enzymes (see the Introduction) are completed through reduction and protonation processes as outlined in Figure 1. More importantly, by direct experimentation, the reduction potential of the superoxide species $[(F_8)Fe^{III}\text{-}(O_2^{\bullet-})]$ (***S***), and the pK_a value for the hydroperoxide analog $[(F_8)Fe^{III}\text{-}(OOH)]$ (***HP***) have been established. With these parameters in hand, the O–H BDFE of ***HP*** could be calculated (73.5 kcal/mol). This work describes the first example of experimentally determined thermodynamics (reduction potential and pK_a) interrelating ***S***, ***P***, and ***HP*** species while also demonstrating the generation of the ferric hydroperoxide complex (***HP***) using an exogenous substrate (TEMPO–H) for HAT by the ferric heme superoxide species (***S***). These results advance the literature concerning the thermodynamics of heme complexes while further showing the utility of synthetic model compounds to provide fundamental insights relevant to reaction cycles of heme enzymes.

As mentioned in Introduction, the peroxide intermediate in catalytic cycle of CYP450 (Scheme 1) is thought to have an end-on (η^1) geometry. Davydov, Sligar, Hoffman, and coworkers[42] detected this end-on bound peroxide intermediate by employing γ-irradiation at cryogenic temperature with P450cam. Thus, one future goal will be research relevant to thermodynamic analysis involving end-on ferric heme peroxide chemistry. We wish to also further assess whether heme or axial ligation modifications may lead to enhancement of the oxidizing capability of a heme-Fe^{II}/O_2 derived adduct.

EXPERIMENTAL SECTION

Materials and Methods. All reagents and solvents purchased and used were of commercially available quality except as noted. Inhibitor-free Tetrahydrofuran (THF) was distilled over Na/benzophenone under argon and deoxygenated with argon before use. Butyronitrile was distilled over sodium carbonate and potassium permanganate and deoxygenated with Ar before use. Cobaltocene was obtained from Sigma Aldrich, sublimed at 75°C, and stored under nitrogen in the glovebox freezer at –30 °C. The 2,6-lutidinium Triflate [(Lu)(H)](OTf) and TEMPO–H(D) were synthesized according to previously published literature procedures.[110–112]

The preparation and handling of air-sensitive compounds were performed under a MBraun Labmaster 130 inert atmosphere (< 1 ppm O_2 and < 1 ppm H_2O) glovebox filled with nitrogen. Dioxygen gas purchased from Airgas and dried through Drierite. $^{18}O_2$ gas was purchased from ICON, Summit, NJ, and $^{16}O_2$ gas was purchased from BOC gases, Murray Hill, NJ.

All UV–vis measurements were carried out using a Hewlett-Packard 8453 diode array spectrophotometer with HP Chemstation software and a Unisoku thermostated cell holder for low-temperature experiments. A 10 mm path length quartz cell cuvette modified with an extended glass neck with a female 14/19 joint, and stopcock was used to perform all UV–vis experiments, as previously described.[99,113,114] ^1H and ^2H NMR spectra were measured on a Bruker 300-MHz NMR spectrometer at ambient or low temperatures. Chemical shifts were reported as δ (ppm) values relative to an internal standard (tetramethylsilane) and the residual solvent proton peaks. Electron paramagnetic resonance (EPR) spectra were recorded with a Bruker EMX spectrometer equipped with a Bruker ER 041 × G microwave bridge and a continuous flow liquid helium cryostat (ESR900) coupled to an Oxford Instruments TC503 temperature controller. Spectra were obtained at 10 K under non-saturating microwave power conditions (ν = 9.428 GHz, microwave power = 0.201 mW, modulation amplitude = 10 G, microwave frequency = 100 kHz, and receiver gain = 5.02 × 10^3).

The compounds $(F_8)Fe^{II}$, and the pyrrole deuterated derivative d_8-$(F_8)Fe^{II}$ were synthesized as previously described.[61,115,116]

UV-vis Spectroscopy.

Generation of $[(F_8)Fe^{III}\text{-}(OOH)]$ (*HP*). After generating complex $[(F_8)Fe^{III}\text{-}(O_2^{2-})]^-$ (***P***),[60] 1 equiv $[(LutH^+)](OTf)$ or [(H)DMF](OTf) was added to the solution of ***P*** to form $[(F_8)Fe^{III}\text{-}(OOH)]$ (***HP***) in THF at –80 °C. UV-vis: λ_{max} = 418 (ε = 157048 M^{-1} cm^{-1}), 536 (ε = 9782.5 M^{-1} cm^{-1}) and 558 (ε = 7322.5 M^{-1} cm^{-1}) nm.

H_2O_2 Quantification by Horseradish Peroxidase (HRP) Test. The spectrophotometric quantification of hydrogen peroxide was carried out by analyzing the intensity of the diammonium 2,2′- azino- bis(3-ethylbenzothiazoline-6-sulfonate)(AzBTS-$(NH_4)_2$) peaks (at different wavelengths to minimize error, Figure S3), which was oxidized by horseradish peroxidase (HRP); this was adapted from published procedures.[72,73] Three stock solutions were prepared: 300 mM sodium phosphate buffer pH 7.0 (solution A), 1 mg/mL AzBTS-$(NH_4)_2$ (solution B) and 4 mg of HRP (type II salt free (Sigma)) with 6.5 mg of sodium azide in 50 mL of water (solution C). 3.0 mL of the desired $[(F_8)Fe^{III}\text{-}(O_2^{2-})]^-$ (***P***) or $[(F_8)Fe^{III}\text{-}(OOH)]$ (***HP***) solution were generated in THF at –80 °C, as previously described. The reaction which is before and after being quenched by adding 100μL of triflic acid (HOTf) solution (2.5 equiv) is subject to the H_2O_2 analysis. Subsequently 100 μL of the cold THF sample solution was removed via a syringe and quickly added to a cuvette containing 1.3 mL of water, 500 μL of solution A, 100 μL of solution B, and 50 μL of solution C (all chilled in an ice bath prior to use). After mixing for 15s, the samples

were allowed to sit at room temperature for ~2 min until full formation of the 418 nm band was observed (Figure S3).

Determination of the reduction potential of [(F_8)Fe^{III}-($O_2^{\bullet-}$)] (*S*). [(F_8)Fe^{III}-($O_2^{\bullet-}$)] (***S***) generated as previously published[61,62] was titrated with 0.25-2 equiv Cr(η-C_6H_6)$_2$ in THF at –80 °C. For each equilibrium mixture, the concentration of each species in solution was measured using the absorption at 434 nm (Table S2). From these equilibrium constants, corresponding reduction potentials were calculated by using the Nernst equation.

Reversibility of [(F_8)Fe^{III}-($O_2^{\bullet-}$)] (*S*) and [(F_8)Fe^{III}-(O_2^{2-})]$^-$ (*P*). In a Schlenk cuvette, the addition of 1 equiv Magic Blue to a solution of [(F_8)Fe^{III}-(O_2^{2-})]$^-$ (***P***) generated from [(F_8)Fe^{III}-($O_2^{\bullet-}$)] (***S***) with 2 equiv Cr(η-C_6H_6)$_2$ in THF at –80 °C leads to the formation of [(F_8)Fe^{III}-($O_2^{\bullet-}$)] (***S***) and again, the addition of 5 equiv Cr(η-C_6H_6)$_2$ gives back [(F_8)Fe^{III}-(O_2^{2-})]$^-$ (***P***) (Figure S6).

Determination of the pK_a of [(F_8)Fe^{III}-(OOH)] (*HP*). In a Schlenk cuvette, [(F_8)Fe^{III}-(OOH)] (***HP***) generated as described above, was titrated by 0.75-3 equiv EtP_2(dma) in THF at –80 °C. For each equilibrium mixture, the concentration of each species in solution was measured using the absorption at 434 nm (Table S4). From these equilibrium constants, the pK_a was calculated.

Reversibility of [(F_8)Fe^{III}-(O_2^{2-})]$^-$ (*P*) and [(F_8)Fe^{III}-(OOH)] (*HP*). In a Schlenk cuvette, the addition of 3 equiv EtP_2(dma) to solution of [(F_8)Fe^{III}-(OOH)] (***HP***) generated as described above, results in the formation of [(F_8)Fe^{III}-(O_2^{2-})]$^-$ (***P***) in THF at –80 °C and again, the addition of 3 equiv [(LutH$^+$)](OTf) gives [(F_8)Fe^{III}-(OOH)] (***HP***) (Figure S8).

Reactivity study of [(F_8)Fe^{III}-($O_2^{\bullet-}$)] (*S*) with TEMPO–H. Excess amount of TEMPO–H (0.4-3.6 mM) was added to the solution of [(F_8)Fe^{III}-($O_2^{\bullet-}$)] (***S***) in THF at –80 °C in a Schlenk cuvette.

Kinetic studies of [(F_8)Fe^{III}-($O_2^{\bullet-}$)] (*S*) with TEMPO–H(D). The substrates TEMPO–H(D) (10, 30, 50, 70, 90 equiv) were added via syringe to a 0.04 mM solution of [(F_8)Fe^{III}-($O_2^{\bullet-}$)] (***S***) and the following UV-vis spectra were recorded (Figure 9). The hydroperoxide band at 418 nm appeared with time and the pseudo-first-order rate plots were observed. The values of k_{obs} were calculated from plots of log[(A_t-A_f)/(A_i-A_f)] vs time (s) (Figure S11, S12). According to this plot of k_{obs} vs [TEMPO–H(D)], the second order rate constant k_2 was obtained in THF at –80 °C (Figure 10).

Resonance Raman Spectroscopy. In the glovebox, 1 mM solutions of (F_8)Fe^{II} in THF were prepared and transferred to rR tube and capped with tightfitting septa. The sample tubes were placed in a cold bath (dry ice/acetone) and oxygenated using $^{16}O_2$ or $^{18}O_2$ gases. The oxygenated samples were set in a cold bath for 10 min and to the cold THF solution of [(F_8)Fe^{III}-($O_2^{\bullet-}$)] (***S***) was added 1 equiv $CoCp_2$ for complex [(F_8)Fe^{III}-(O_2^{2-})]$^-$ (***P***). Subsequently, 1 equiv [(LutH$^+$)](OTf) was added for complex [(F_8)Fe^{III}-(OOH)] (***HP***). Then, the sample tubes were frozen in liquid N_2 and sealed by flame. Resonance Raman samples were excited at 413 nm, using a Coherent I90C-K Kr^+ ion laser while the sample was immersed in a liquid nitrogen cooled (77 K) EPR finger Dewar (Wilmad). Power was ~2 mW at the sample, which was continuously rotated to minimize photodecomposition. The spectra were recorded using a Spex 1877 CP triple monochromator, and detected by an Andor Newton CCD cooled to –80 °C.

Electron Paramagnetic Resonance (EPR) Spectroscopy. In a glovebox, 1 mM solutions of (F_8)Fe^{II} in THF were prepared and transferred to EPR tube and capped with tightfitting septa. The sample tubes were placed in a cold bath (dry ice/acetone) and oxygenated. The oxygenated samples were set in a cold bath for 10 min and to the cold THF solution of [(F_8)Fe^{III}-($O_2^{\bullet-}$)] (***S***) was added 1 equiv $CoCp_2$ for complex [(F_8)Fe^{III}-(O_2^{2-})]$^-$ (***P***). Subsequently, 1 equiv [(LutH$^+$)](OTf) was added for complex [(F_8)Fe^{III}-(OOH)] (***HP***). Then, the sample tubes were frozen in liquid N_2.

For EPR data for the reaction of [(F_8)Fe^{III}-($O_2^{\bullet-}$)] (***S***) with TEMPO–H, 10 equiv TEMPO–H was added to the 1mM solution of ***S*** generated as described above. The tube was left at –80 °C for 1 hour 30 minutes and then frozen in liquid nitrogen.

ASSOCIATED CONTENT

Supporting information

For [(F_8)Fe^{II}], ***S***, ***P*** and ***HP***, associated spectroscopic data (^{2}H-NMR, EPR, rRaman and UV-vis), kinetic data for the reaction of ***S*** with TEMPO–H(D), details concerning H_2O_2 quantification, calculations relevant to reduction potential and pK_a experiments, control experimental details, and tabulated data from the literature on (i) theoretically considered and computed thermodynamics of ferric-heme superoxide reduction potential, ferric heme hydroperoxide pK_a and OO–H BDFE, and (ii) non-heme first-row transition metal ion superoxide complex kinetics of reaction with TEMPO–H(D). This material is available free of charge via the internet at http://pubs.acs.org

AUTHOR INFORMATION

Corresponding Authors

karlin@jhu.edu
edward.solomon@stanford.edu

Notes

The authors declare no competing financial interest.

ORCID

Hyun Kim: 0000-0001-9823-6457
Savita K. Sharma: 0000-0001-5489-8416
Andrew W. Schaefer: 0000-0001-6565-920X
Edward I. Solomon: 0000-0003-0291-3199
Kenneth D. Karlin: 0000-0002-5675-7040

ACKNOWLEDGMENT

This research was supported by the USA National Institutes of Health (GM60353 to K.D.K. and GM040392 to E.I.S.).

REFERENCES

(1) Meunier, B.; de Visser, S. P.; Shaik, S. Mechanism of Oxidation Reactions Catalyzed by Cytochrome P450 Enzymes. *Chem. Rev.* **2004**, *104*, 3947–3980.

(2) Denisov, I. G.; Makris, T. M.; Sligar, S. G.; Schlichting, I. Structure and Chemistry of Cytochrome P450. *Chem. Rev.* **2005**, *105*, 2253–2277.

(3) Shaik, S.; Kumar, D.; de Visser, S. P.; Altun, A.; Thiel, W. Theoretical Perspective on the Structure and Mechanism of Cytochrome P450 Enzymes. *Chem. Rev.* **2005**, *105*, 2279–2328.

(4) Ortiz De Montellano, P. R. Hydrocarbon Hydroxylation by

Cytochrome P450 Enzymes. *Chem. Rev.* **2010**, *110*, 932–948.

(5) Shaik, S.; Cohen, S.; Wang, Y.; Chen, H.; Kumar, D.; Thiel, W. P450 Enzymes: Their Structure, Reactivity, and Selectivity-Modeled by QM/MM Calculations. *Chem. Rev.* **2010**, *110*, 949–1017.

(6) Poulos, T. L. Heme Enzyme Structure and Function. *Chem. Rev.* **2014**, *114*, 3919–3962.

(7) McQuarters, A. B.; Wolf, M. W.; Hunt, A. P.; Lehnert, N. 1958-2014: After 56 Years of Research, Cytochrome P450 Reactivity Is Finally Explained. *Angew. Chem., Int. Ed.* **2014**, *53*, 4750–4752.

(8) Adam, S. M.; Wijeratne, G. B.; Rogler, P. J.; Diaz, D. E.; Quist, D. A.; Liu, J. J.; Karlin, K. D. Synthetic Fe/Cu Complexes: Toward Understanding Heme-Copper Oxidase Structure and Function. *Chem. Rev.* **2018**, *118*, 10840–11022.

(9) Huang, X.; Groves, J. T. Oxygen Activation and Radical Transformations in Heme Proteins and Metalloporphyrins. *Chem. Rev.* **2018**, *118*, 2491–2553.

(10) Dubey, K. D.; Shaik, S. Cytochrome P450-The Wonderful Nanomachine Revealed through Dynamic Simulations of the Catalytic Cycle. *Acc. Chem. Res.* **2019**, *52*, 389–399.

(11) Goto, Y.; Wada, S.; Morishima, I.; Watanabe, Y. Reactivity of Peroxoiron(III) Porphyrin Complexes: Models for Deformylation Reactions Catalyzed by Cytochrome P-450. *J. Inorg. Biochem.* **1998**, *69*, 241–247.

(12) Guengerich, F. P. Cytochrome P450 and Chemical Toxicology. *Chem. Res. Toxicol.* **2008**, *21*, 70–83.

(13) Newcomb, M.; Halgrimson, J. A.; Horner, J. H.; Wasinger, E. C.; Chen, L. X.; Sligar, S. G. X-Ray Absorption Spectroscopic Characterization of a Cytochrome P450 Compound II Derivative. *Proc. Natl. Acad. Sci. U. S. A.* **2008**, *105*, 8179–8184.

(14) Karlin, K. D. Model Offers Intermediate Insight. *Nature* **2010**, *463*, 168–169.

(15) Poulos, T. L.; Finzel, B. C.; Howard, A. J. High-Resolution Crystal Structure of Cytochrome P450cam. *J. Mol. Biol.* **1987**, *195*, 687–700.

(16) Schlichting, I.; Jung, C.; Schulze, H. Crystal Structure of Cytochrome P-450cam Complexed with the (1S)-camphor Enantiomer. *FEBS Lett.* **1997**, *415*, 253–257.

(17) Lai, W.; Chen, H.; Cho, K.-B.; Shaik, S. External Electric Field Can Control the Catalytic Cycle of Cytochrome P450cam: A QM/MM Study. *J. Phys. Chem. Lett.* **2010**, *1*, 2082–2087.

(18) Lai, W.; Shaik, S. Can Ferric-Superoxide Act as a Potential Oxidant in $P450_{Cam}$? QM/MM Investigation of Hydroxylation, Epoxidation, and Sulfoxidation. *J. Am. Chem. Soc.* **2011**, *133*, 5444–5452.

(19) Ogliaro, F.; de Visser, S. P.; Cohen, S.; Sharma, P. K.; Shaik, S. Searching for the Second Oxidant in the Catalytic Cycle of Cytochrome P450: A Theoretical Investigation of the Iron(III)-Hydroperoxo Species and Its Epoxidation Pathways. *J. Am. Chem. Soc.* **2002**, *124*, 2806–2817.

(20) de Visser, S. P.; Valentine, J. S.; Nam, W. A Biomimetic Ferric Hydroperoxo Porphyrin Intermediate. *Angew. Chem., Int. Ed.* **2010**, *49*, 2099–2101.

(21) Loew, G. H.; Harris, D. L. Role of the Heme Active Site and Protein Environment in Structure, Spectra, and Function of the Cytochrome P450s. *Chem. Rev.* **2000**, *100*, 407–419.

(22) Davydov, R.; Macdonald, I. D. G.; Makris, T. M.; Sligar, S. G.; Hoffman, B. M. EPR and ENDOR of Catalytic Intermediates in Cryoreduced Native and Mutant Oxy-Cytochromes P450cam: Mutation-Induced Changes in the Proton Delivery System. *J. Am. Chem. Soc.* **1999**, *121*, 10654–10655.

(23) Sono, M.; Roach, M. P.; Coulter, E. D.; Dawson, J. H. Heme-Containing Oxygenases. *Chem. Rev.* **1996**, *96*, 2841–2888.

(24) Huang, X.; Groves, J. T. Beyond Ferryl-Mediated Hydroxylation: 40 Years of the Rebound Mechanism and C–H Activation. *J. Biol. Inorg. Chem.* **2017**, *22*, 185–207.

(25) Garcia-Serres, R.; Davydov, R. M.; Matsui, T.; Ikeda-Saito, M.; Hoffman, B. M.; Huynh, B. H. Distinct Reaction Pathways Followed upon Reduction of Oxy-Heme Oxygenase and Oxy-Myoglobin as Characterized by Mössbauer Spectroscopy. *J. Am. Chem. Soc.* **2007**, *129*, 1402–1412.

(26) Matsui, T.; Unno, M.; Ikeda-saito, M. Heme Oxygenase Reveals Its Strategy For Catalyzing Three Successive Oxygenation Reactions. *Acc. Chem. Res.* **2010**, *43*, 240–247.

(27) Matsui, T.; Nambu, S.; Goulding, C. W.; Takahashi, S.; Fujii, H.; Ikeda-Saito, M. Unique Coupling of Mono- and Dioxygenase Chemistries in a Single Active Site Promotes Heme Degradation. *Proc. Natl. Acad. Sci. U. S. A.* **2016**, *113*, 3779–3784.

(28) Zhu, Y.; Silverman, R. B. Revisiting Heme Mechanisms. A Perspective on the Mechanisms of Nitric Oxide Synthase (NOS), Heme Oxygenase (HO), and Cytochrome P450s (CYP450s). *Biochemistry* **2008**, *47*, 2231–2243.

(29) Lehnert, N.; Berto, T. C.; Galinato, M. G. I.; Goodrich, L. E. The Role of Heme-Nitrosyls in the Biosynthesis, Transport, Sensing, and Detoxification of Nitric Oxide (NO) in Biological Systems: Enzymes and Model Complexes. *Handbook of Porphyrin Science*; World Scientific Publishing Company: Singapore, **2011**, Vol. 14, pp 1–247 (Chapter 63).

(30) Gantt, S. L.; Denisov, I. G.; Grinkova, Y. V.; Sligar, S. G. The Critical Iron-Oxygen Intermediate in Human Aromatase. *Biochem. Biophys. Res. Commun.* **2009**, *387*, 169–173.

(31) Mak, P. J.; Gregory, M. C.; Denisov, I. G.; Sligar, S. G.; Kincaid, J. R. Unveiling the Crucial Intermediates in Androgen Production. *Proc. Natl. Acad. Sci. U. S. A.* **2015**, *112*, 15856–15861.

(32) Mak, P. J.; Duggal, R.; Denisov, I. G.; Gregory, M. C.; Sligar, S. G.; Kincaid, J. R. Human Cytochrome CYP17A1: The Structural Basis for Compromised Lyase Activity with 17-Hydroxyprogesterone. *J. Am. Chem. Soc.* **2018**, *140*, 7324–7331.

(33) Denisov, I. G.; Makris, T. M.; Sligar, S. G. Formation and Decay of Hydroperoxo-Ferric Heme Complex in Horseradish Peroxidase Studied by Cryoradiolysis. *J. Biol. Chem.* **2002**, *277*, 42706–42710.

(34) Veitch, N. C. Horseradish Peroxidase: A Modern View of a Classic Enzyme. *Phytochemistry* **2004**, *65*, 249–259.

(35) Denisov, I. G.; Dawson, J. H.; Hager, L. P.; Sligar, S. G. The Ferric-Hydroperoxo Complex of Chloroperoxidase. *Biochem. Biophys. Res. Commun.* **2007**, *363*, 954–958.

(36) Wang, X.; Ullrich, R.; Hofrichter, M.; Groves, J. T. Heme-Thiolate Ferryl of Aromatic Peroxygenase Is Basic and Reactive. *Proc. Natl. Acad. Sci. U. S. A.* **2015**, *112*, 3686–3691.

(37) Lewis-Ballester, A.; Forouhar, F.; Kim, S. M.; Lew, S.; Wang, Y.; Karkashon, S.; Seetharaman, J.; Batabyal, D.; Chiang, B. Y.; Hussain, M.; ; Correia, M. A.; Yeh, S. R.; Tong, L. Molecular Basis for Catalysis and Substrate-Mediated Cellular Stabilization of Human Tryptophan 2,3-Dioxygenase. *Sci. Rep.* **2016**, *6*, 35169.

(38) Recent resonant inelastic X-ray scattering (RIXS) analyses have shown that the electronic structure more closely fits to an Fe^{II}–(O_2) description for a model system (the "oxy picket-fence porphyrin"), while oxy-hemoglobin has more Fe^{III}-$(O_2^{\bullet-})$ character (although not fully to the low-spin ferric level). Yan, J. J.; Kroll, T.; Baker, M. L.; Wilson, S. A.; Decréau, R.; Lundberg, M.; Sokaras, D.; Glatzel, P.; Hedman, B.; Hodgson, K. O.; Solomon, E. I. *Proc. Natl. Acad. Sci. U. S. A.* **2019**, *116*, 2854–2859.

(39) Denisov, I. G.; Makris, T. M.; Sligar, S. G. Cryotrapped Reaction Intermediates of Cytochrome P450 Studied by Radiolytic Reduction with Phosphorus-32. *J. Biol. Chem.* **2001**, *276*, 11648–11652.

(40) Davydov, R.; Satterlee, J. D.; Fujii, H.; Sauer-Masarwa, A.; Busch, D. H.; Hoffman, B. M. A Superoxo-Ferrous State in a Reduced Oxy-Ferrous Hemoprotein and Model Compounds. *J. Am. Chem. Soc.* **2003**, *125*, 16340–16346.

(41) Davydov, R.; Perera, R.; Jin, S.; Yang, T. C.; Bryson, T. A.; Sono, M.; Dawson, J. H.; Hoffman, B. M. Substrate Modulation of the Properties and Reactivity of the Oxy-Ferrous and Hydroperoxo-Ferric Intermediates of Cytochrome P450cam as Shown by Cryoreduction-EPR/ENDOR Spectroscopy. *J. Am. Chem. Soc.* **2005**, *127*, 1403–1413.

(42) Davydov, R.; Makris, T. M.; Kofman, V.; Werst, D. E.; Sligar, S. G.; Hoffman, B. M. Hydroxylation of Camphor by Reduced Oxy-Cytochrome P450cam : Mechanistic Implications of EPR and ENDOR Studies of Catalytic Intermediates in Native and Mutant Enzymes. *J. Am. Chem. Soc.* **2001**, *123*, 1403–1415.

(43) Collman, J. P.; Gagnet, R. R.; Reed, C. A.; Robinson, W. T.; Rodley, G. A. Structure of an Iron (II) Dioxygen Complex ; A Model for Oxygen Carrying Hemeproteins. *Proc. Natl. Acad. Sci. U. S. A.* **1974**, *71*, 1326–1329.

(44) Singha, A.; Dey, A. Hydrogen Atom Abstraction by Synthetic Heme Ferric Superoxide and Hydroperoxide Species. *Chem. Commun.* **2019**, *55*, 5591–5594.

(45) Momenteau, M.; Reed, C. A. Synthetic Heme Dioxygen Complexes. *Chem. Rev.* **1994**, *94*, 659–698.

(46) Collman, J. P.; Sunderland, C. J.; Berg, K. E.; Vance, M. A.; Solomon, E. I. Spectroscopic Evidence for a Heme-Superoxide/Cu(I) Intermediate in a Functional Model of Cytochrome *c* Oxidase. *J. Am. Chem. Soc.* **2003**, *125*, 6648–6649.

(47) Liu, J.-G.; Naruta, Y.; Tani, F. A Functional Model of the Cytochrome *c* Oxidase Active Site: Unique Conversion of a Heme–μ-Peroxo–Cu^{II} Intermediate into Heme– Superoxo/Cu^{I}. *Angew. Chem., Int. Ed.* **2005**, *44*, 1836–1840.

(48) Liu, J.-G.; Ohta, T.; Yamaguchi, S.; Ogura, T.; Sakamoto, S.; Maeda, Y.; Naruta, Y. Spectroscopic Characterization of a Hydroperoxo-Heme Intermediate: Conversion of a Side-on Peroxo to an End-on Hydroperoxo Complex. *Angew. Chem., Int. Ed.* **2009**, *48*, 9262–9267.

(49) Liu, J.-G.; Shimizu, Y.; Ohta, T.; Naruta, Y. Formation of an End-on Ferric Peroxo Intermediate upon One-Electron Reduction of a Ferric Superoxo Heme. *J. Am. Chem. Soc.* **2010**, *132*, 3672–3673.

(50) Li, Y.; Sharma, S. K.; Karlin, K. D. New Heme-Dioxygen and Carbon Monoxide Adducts Using Pyridyl or Imidazolyl Tailed Porphyrins. *Polyhedron* **2013**, *58*, 190–196.

(51) Nagaraju, P.; Ohta, T.; Liu, J.-G.; Ogura, T.; Naruta, Y. The Secondary Coordination Sphere Controlled Reactivity of a Ferric-Superoxo Heme: Unexpected Conversion to a Ferric Hydroperoxo Intermediate by Reaction with a High-Spin Ferrous Heme. *Chem. Commun.* **2016**, *52*, 7213–7216.

(52) Kim, H.; Sharma, S. K.; Schaefer, A. W.; Solomon, E. I.; Karlin, K. D. Heme–Cu Binucleating Ligand Supports Heme/O_2 and Fe^{II}–Cu^{I}/O_2 Reactivity Providing High- and Low-Spin Fe^{III}–Peroxo–Cu^{II} Complexes. *Inorg. Chem.* **2019**, *58*, 15423-15432.

(53) Vaz, A. D. N.; McGinnity, D. F.; Coon, M. J. Epoxidation of Olefins by Cytochrome P450: Evidence from Site-Specific Mutagenesis for Hydroperoxo-Iron as an Electrophilic Oxidant. *Proc. Natl. Acad. Sci. U. S. A.* **1998**, *95*, 3555–3560.

(54) Newcomb, M.; Shen, R.; Choi, S.-Y.; Toy, P. H.; Hollenberg, P. F.; Vaz, A. D. N.; Coon, M. J. Cytochrome P450-Catalyzed Hydroxylation of Mechanistic Probes That Distinguish between Radicals and Cations. Evidence for Cationic but Not for Radical Intermediates. *J. Am. Chem. Soc.* **2000**, *122*, 2677–2686.

(55) Jin, S.; Makris, T. M.; Bryson, T. A.; Sligar, S. G.; Dawson, J. H. Epoxidation of Olefins by Hydroperoxo-Ferric Cytochrome P450. *J. Am. Chem. Soc.* **2003**, *125*, 3406–3407.

(56) Fukuzumi, S.; Lee, Y.-M.; Nam, W. Structure and Reactivity of the First-Row d-Block Metal-Superoxo Complexes. *Dalt. Trans.* **2019**, *48*, 9469–9489.

(57) Noh, H.; Cho, J. Synthesis, Characterization and Reactivity of Non-Heme 1st Row Transition Metal-Superoxo Intermediates. *Coord. Chem. Rev.* **2019**, *382*, 126–144.

(58) Davydov, R.; Hoffman, B. M. Active Intermediates in Heme Monooxygenase Reactions as Revealed by Cryoreduction/Annealing, EPR/ENDOR Studies. *Arch. Biochem. Biophys.* **2011**, *507*, 36–43.

(59) W Warren, J. J.; Tronic, T. A.; Mayer, J. M. Thermochemistry of Proton-Coupled Electron Transfer Reagents and Its Implications. *Chem. Rev.* **2010**, *110*, 6961–7001.

(60) Chufán, E. E.; Karlin, K. D. An Iron-Peroxo Porphyrin Complex : New Synthesis and Reactivity Toward a Cu(II) Complex Giving a Heme-Peroxo-Copper Adduct. *J. Am. Chem. Soc.* **2003**, *125*, 16160–16161.

(61) Ghiladi, R. A.; Kretzer, R. M.; Guzei, I.; Rheingold, A. L.; Neuhold, Y.-M.; Hatwell, K. R.; Zuberbühler, A. D.; Karlin, K. D. (F_8TPP)Fe^{II}/O_2 Reactivity Studies {F_8TPP = Tetrakis(2,6-difluorophenyl)porphyrinate(2−)}: Spectroscopic (UV−Visible and NMR) and Kinetic Study of Solvent-Dependent (Fe/O_2 = 1:1 or 2:1) Reversible O_2-Reduction and Ferryl Formation. *Inorg. Chem.* **2001**, *40*, 5754–5767.

(62) Kim, E.; Helton, M. E.; Wasser, I. M.; Karlin, K. D.; Lu, S.; Huang, H.-w.; Moënne-Loccoz, P.; Incarvito, C. D.; Rheingold, A. L.; Honecker, M.; Kaderli, S.; Zuberbühler, A. D. Superoxo, μ-peroxo, and μ-oxo Complexes from Heme/O_2 and Heme-Cu/O_2 Reactivity: Copper Ligand Influences in Cytochrome *c* Oxidase Models. *Proc. Natl. Acad. Sci. U. S. A.* **2003**, *100*, 3623–3628.

(63) McCandlish, E.; Mikszta, A. R.; Nappa, M.; Sprenger, A. Q.; Valentine, J. S.; Stong, J. D.; Spiro, T. G. Reactions of Superoxide with Iron Porphyrins in Aprotic Solvents. A High Spin Ferric Porphyrin Peroxo Complex. *J. Am. Chem. Soc.* **1980**, *102*, 4268–4271.

(64) Selke, M.; Sisemore, M. F.; Valentine, J. S. The Diverse Reactivity of Peroxy Ferric Porphyrin Complexes of Electron-Rich and Electron-Poor Porphyrins. *J. Am. Chem. Soc.* **1996**, *118*, 2008–2012.

(65) TPP = meso-tetraphenylporphyrin, OEP = octaethylporphyrin.

(66) VanAtta, R. B.; Strouse, C. E.; Hanson, L. K.; Valentine, J. S. [Peroxotetraphenylporphinato]Manganese(III) and [Chlorotetraphenylporphinato]Manganese(II) Anions. Syntheses, Crystal Structures, and Electronic Structures. *J. Am. Chem. Soc.* **1987**, *109*, 1425–1434.

(67) There do exist S = 3/2 six-coordinate [(porphyrinate)Fe^{III}-(X)(X')] complexes, where X and X' are weak ligands (e.g., ethanol, H_2O, THF) not involving a side-on bound peroxo ligand. (a) Simonato, J.-P.; Pécaut, J.; Le Pape, L.; Oddou, J.-L.; Jeandey, C.; Shang, M.; Scheidt, W. R.; Wojaczyński, J.; Wo łowiec, S.; Latos-Grażyński, L.; Marchon, J.-C. An Integrated Approach to the Mid-Spin State (S= 3/2) in Six-Coordinate Iron(III) Chiroporphyrins. *Inorg. Chem*. **2000**, *39*, 3978–3987. (b) Ikeue, T.; Ohgo, Y.; Yamaguchi, T.; Takahashi, M.; Takeda, M.; Nakamura, M. Saddle-Shaped Six-Coordinated Iron(III) Porphyrin Complexes Showing a Novel Spin Crossover between S = 1/2 and S = 3/2 Spin States. *Angew. Chem., Int. Ed.* **2001**, *40*, 2617–2620.

(68) Neese, F.; Solomon, E. I. Detailed Spectroscopic and Theoretical Studies on [Fe(EDTA)(O_2)]$^{3-}$: Electronic Structure of the Side-on Ferric-Peroxide Bond and Its Relevance to Reactivity. *J. Am. Chem. Soc.* **1998**, *120*, 12829–12848.

(69) Simaan, A. J.; Döpner, S.; Banse, F.; Bourcier, S.; Bouchoux, G.; Boussac, A.; Hildebrandt, P.; Girerd, J.-J. Fe^{III}-Hydroperoxo and Peroxo Complexes with Aminopyridyl Ligands and the Resonance Raman Spectroscopic Identification of the Fe-O and O-O Stretching Modes. *Eur. J. Inorg. Chem.* **2000**, 1627–1633.

(70) Roelfes, G.; Vrajmasu, V.; Chen, K.; Ho, R. Y. N.; Rohde, J.-U.; Zondervan, C.; la Crois, R. M.; Schudde, E. P.; Lutz, M.; Spek, A. L.; Hage, R.; Feringa, B. L.; Münck, E.; Que, L. End-on and Side-on Peroxo Derivatives of Non-Heme Iron Complexes with Pentadentate Ligands: Models for Putative Intermediates in Biological Iron/Dioxygen Chemistry. *Inorg. Chem.* **2003**, *42*, 2639–2653.

(71) Van Wart, H. E.; Zimmer, J. Resonance Raman Evidence for the Activation of Dioxygen in Horseradish Oxyperoxidase. *J. Biol. Chem.* **1985**, *260*, 8372–8377.

(72) Peterson, R. L.; Ginsbach, J. W.; Cowley, R. E.; Qayyum, M. F.; Himes, R. A.; Siegler, M. A.; Moore, C. D.; Hedman, B.; Hodgson, K. O.; Fukuzumi, S.; Solomon, E. I.; Karlin, K. D. Stepwise Protonation and Electron-Transfer Reduction of a Primary Copper-Dioxygen Adduct. *J. Am. Chem. Soc.* **2013**, *135*, 16454–16467.

(73) Adam, S. M.; Garcia-Bosch, I.; Schaefer, A. W.; Sharma, S. K.; Siegler, M. A.; Solomon, E. I.; Karlin, K. D. Critical Aspects of Heme–Peroxo–Cu Complex Structure and Nature of Proton Source Dictate Metal–O_{Peroxo} Breakage versus Reductive O–O Cleavage Chemistry. *J . Am. Chem. Soc.* **2017**, *139*, 472–481.

(74) Carver, C. T.; Matson, B. D.; Mayer, J. M. Electrocatalytic Oxygen Reduction by Iron Tetra-arylporphyrins Bearing Pendant Proton Relays. *J. Am. Chem. Soc.* **2012**, *134*, 5444–5447.

(75) Tajima, K.; Oka, S.; Edo, T.; Miyake, S.; Mano, H.; Mukai, K.; Sakurai, H.; Ishizu, K. Optical Absorption and EPR studies on a Six-coordinate Iron(III)-tetramesitylporphyrin-Hydorgen Peroxide complex Having a Nitrogenous Axial Ligand. *J. Chem. Soc., Chem. Commun.* **1995**, 1507–1508.

(76) Oliveira, R.; Zouari, W.; Herrero, C.; Banse, F.; Schöllhorn, B.; Fave, C.; Anxolabéhère-Mallart, E. Characterization and Subsequent Reactivity of an Fe-Peroxo Porphyrin Generated by Electrochemical Reductive Activation of O_2. *Inorg. Chem.* **2016**, *55*, 12204–12210.

(77) Tajima, K.; Shigematsu, M.; Jinno, J.; Ishizu, K.; Ohya-Nishiguchic, H. Generation of Fe^{III}OEP-Hydrogen Peroxide Complex (OEP = Octaethylporphyrinato) by Reduction of Fe^{II}OEP-O_2 with Ascorbic Acid Sodium Salt. *J. Chem. Soc., Chem. Commun.,* **1990**, 144–145.

(78) Davydov, R. M.; Yoshida, T.; Ikeda-Saito, M.; Hoffman, B. M. Hydroperoxy-Heme Oxygenase Generated by Cryoreduction Catalyzes the Formation of α-*meso*-Hydroxyheme as Detected by EPR and ENDOR. *J. Am. Chem. Soc.* **1999**, *121*, 10656–10657.

(79) Ibrahim, M.; Denisov, I. G.; Makris, T. M.; Kincaid, J. R.; Sligar, S. G. Resonance Raman Spectroscopic Studies of Hydroperoxo-Myoglobin at Cryogenic Temperatures. *J. Am. Chem. Soc.* **2003**, *125*, 13714–13718.

(80) Sengupta, K.; Chatterjee, S.; Samanta, S.; Dey, A. Direct Observation of Intermediates Formed during Steady-State Electrocatalytic O_2 Reduction by Iron Porphyrins. *Proc. Natl. Acad. Sci. U. S. A.* **2013**, *110*, 8431–8436.

(81) Mak, P. J.; Denisov, I. G.; Victoria, D.; Makris, T. M.; Deng, T.; Sligar, S. G.; Kincaid, J. R. Resonance Raman Detection of the Hydroperoxo Intermediate in the Cytochrome P450 Enzymatic Cycle. *J. Am. Chem. Soc.* **2007**, *129*, 6382–6383.

(82) Denisov, I. G.; Mak, P. J.; Makris, T. M.; Sligar, S. G.; Kincaid, J. R. Resonance Raman Characterization of the Peroxo and Hydroperoxo

Intermediates in Cytochrome P450. *J. Phys. Chem. A* **2008**, *112*, 13172–13179.

(83) Schaefer, A. W.; Ehudin, M. A.; Quist, D. A.; Tang, J. A.; Karlin, K. D.; Solomon, E. I. Spin Interconversion of Heme-Peroxo-Copper Complexes Facilitated by Intramolecular Hydrogen-Bonding Interactions. *J. Am. Chem. Soc.* **2019**, *141*, 4936–4951.

(84) Tajima, K.; Jinno, J.; Ishizu, K.; Sakurai, H.; Ohya-Nishiguchi, H. Direct Evidence of Heme-*tert*-Butyl Peroxide Adduct Formation Demonstrated by Simultaneous ESR and Optical Measurements. *Inorg. Chem.* **1989**, *28*, 709–715.

(85) Connelly, N. G.; Geiger, W. E. Chemical Redox Agents for Organometallic Chemistry. *Chem. Rev.* **1996**, *96*, 877–910.

(86) Our statements concerning relative redox potentials for the synthetic heme-superoxide complexes discussed are rough, since experimental or computationally derived redox potentials are from different solvents and approximations are made in converting E°' values from one reference electrode to another (e.g., $Fc^{+/0}$, SCE, SHE).

(87) Garrido, G.; Koort, E.; Ràfols, C.; Bosch, E.; Rodima, T.; Leito, I.; Rosés, M. Acid-Base Equilibria in Nonpolar Media . Absolute pK_a Scale of Bases in Tetrahydrofuran. *J. Org. Chem.* **2006**, *71*, 9062–9067.

(88) Bordwell, F. G.; Cheng, J.-P.; Harrelson, J. A. Homolytic Bond Dissociation Energies in Solution from Equilibrium Acidity and Electrochemical Data. *J. Am. Chem. Soc.* **1988**, *110*, 1229–1231.

(89) Quist, D. A.; Ehudin, M. A.; Schaefer, A. W.; Schneider, G. L.; Solomon, E. I.; Karlin, K. D. Ligand Identity-Induced Generation of Enhanced Oxidative Hydrogen Atom Transfer Reactivity for a $Cu^{II}_2(O_2^{\bullet-})$ Complex Driven by Formation of a $Cu^{II}_2(^{-}OOH)$ Compound with a Strong O–H Bond. *J. Am. Chem. Soc.* **2019**, *141*, 12682–12696.

(90) For Naruta's superstructured ferric heme superoxide, peroxide and hydroperoxide complexes[40] (with or without a H-bonding moiety to interact with the O_2-derived fragment) (Figure S7), theoretical computations were carried out and superoxide-to-peroxide reduction potentials and hydroperoxide/peroxide pK_a values were provided; however BDFE's for the ferric heme hydroperoxide complexes were not evaluated.

(91) Chung, L. W.; Li, X.; Hirao, H.; Morokuma, K. Comparative Reactivity of Ferric-Superoxo and Ferryl-Oxo Species in Heme and Non-Heme Complexes. *J. Am. Chem. Soc.* **2011**, *133*, 20076–20079.

(92) Latifi, R.; Tahsini, L.; Nam, W.; de Visser, S. P. Regioselectivity of Aliphatic *versus* Aromatic Hydroxylation by a Nonheme Iron(II)-Superoxo Complex. *Phys. Chem. Chem. Phys.* **2012**, *14*, 2518–2524.

(93) Gordon, J. B.; Vilbert, A. C.; Siegler, M. A.; Lancaster, K. M.; Moënne-Loccoz, P.; Goldberg, D. P. A Nonheme Thiolate-Ligated Cobalt Superoxo Complex: Synthesis and Spectroscopic Characterization, Computational Studies, and Hydrogen Atom Abstraction Reactivity. *J. Am. Chem. Soc.* **2019**, *141*, 3641–3653.

(94) Kindermann, N.; Günes, C.-J.; Dechert, S.; Meyer, F. Hydrogen Atom Abstraction Thermodynamics of a μ-1,2-Superoxo Dicopper(II) Complex. *J. Am. Chem. Soc.* **2017**, *139*, 9831–9834.

(95) Dhar and Tolman[77a] determined BDE = 90 kcal/mol for an O–H bond of a Cu^{III}-aqua complex, while Kieber-Emmons and coworkers[77b] determined that a mono-hydroxo-bridged dicopper(II) complex possesses an O–H BDE of 77 kcal/mol; this species derives from HAT chemistry of the corresponding μ-oxo dicopper(II) complex. Mayer and coworkers[77c,d,e] reported on several cases of coupled proton-electron transfer (CPET) not involving O–H bond reactions; here, heme or non-heme iron(III) compounds reacting with a hydrogen-atom donor substrate react such that an electron transfers to the iron while the proton transfers to a basic site on the ligand periphery. (a) Dhar, D.; Tolman, W. B. Hydrogen Atom Abstraction from Hydrocarbons by a Copper(III)-Hydroxide Complex. *J. Am. Chem. Soc.* **2015**, *137*, 1322-1329. (b) Ali, G.; VanNatta, P. E.; Ramirez, D. A.; Light, K. M.; Kieber-Emmons, M. T. Thermodynamics of a μ-oxo Dicopper(II) Complex for Hydrogen Atom Abstraction. *J Am. Chem. Soc.* **2017**, *139*, 18448-18451. (c) Roth, J. P.; Lovell, S.; Mayer, J. M. Intrinsic Barriers for Electron and Hydrogen Atom Transfer Reactions of Biomimetic Iron Complexes. *J. Am. Chem. Soc.* **2000**, *122*, 5486-5498. (d) Mader, E. A.; Davidson, E. R.; Mayer, J. M. Large Gournd-State Entropy Changes for Hydrogen Atom Transfer Reactions of Iron Complexes. *J. Am. Chem. Soc.* **2007**, *129*, 5153-5166. (e) Warren, J. J.; Mayer, J. M. Proton-Coupled Electron Trnasfer Reactions at a Heme-Propionate in an Iron-Protoporphyrin-IX Model Compound. *J. Am. Chem. Soc.* **2011**, *133*, 8544-8551.

(96) Perhaps Naruta and coworkers did not address the issue of BDFE's with their data because they did not explore possible HAT chemistry with their corresponding ferric heme superoxide complexes.

(97) Zhu, X.-Q.; Zhang, M.-T.; Yu, A.; Wang, C.-H.; Cheng, J.-P. Hydride , Hydrogen Atom , Proton , and Electron Transfer Driving Forces of Various Five-Membered Heterocyclic Organic Hydrides and Their Reaction Intermediates in Acetonitrile. *J . Am. Chem. Soc.* **2008**, *130*, 2501–2516.

(98) Corsi, D. M.; Murthy, N. N.; Young, V. G.; Karlin, K. D. Synthesis, Structure, and Solution NMR Studies of Cyanide-Copper(II) and Cyanide-Bridged Iron(III)-Copper(II) Complexes. *Inorg. Chem.* **1999**, *38*, 848–858.

(99) Sharma, S. K.; Schaefer, A. W.; Lim, H.; Matsumura, H.; Moënne-Loccoz, P.; Hedman, B.; Hodgson, K. O.; Solomon, E. I.; Karlin, K. D. A Six-Coordinate Peroxynitrite Low-Spin Iron(III) Porphyrinate Complex—The Product of the Reaction of Nitrogen Monoxide ($\cdot NO_{(g)}$) with a Ferric-Superoxide Species. *J. Am. Chem. Soc.* **2017**, *139*, 17421–17430.

(100) Porter, T. R.; Mayer, J. M. Radical Reactivity of the Fe(III)/(II) Tetramesitylporphyrin Couple: Hydrogen Atom Transfer, Oxyl Radical Dissociation, and Catalytic Disproportionation of a Hydroxylamine. *Chem. Sci.* **2014**, *5*, 372–380.

(101) Tano, T.; Okubo, Y.; Kunishita, A.; Kubo, M.; Sugimoto, H.; Fujieda, N.; Ogura, T.; Itoh, S. Redox Properties of a Mononuclear Copper(II)-Superoxide Complex. *Inorg. Chem.* **2013**, *52*, 10431–10437.

(102) Bailey, W. D.; Dhar, D.; Cramblitt, A. C.; Tolman, W. B. Mechanistic Dichotomy in Proton-Coupled Electron-Transfer Reactions of Phenols with a Copper Superoxide Complex. *J. Am. Chem. Soc.* **2019**, *141*, 5470–5480.

(103) Lin, Y.-H.; Cramer, H. H.; van Gastel, M.; Tsai, Y.-H.; Chu, C.-Y.; Kuo, T.-S.; Lee, I.-R.; Ye, S.; Bill, E.; Lee, W.-Z. Mononuclear Manganese(III) Superoxo Complexes: Synthesis, Characterization, and Reactivity. *Inorg. Chem.* **2019**, *58*, 9756–9765.

(104) Wind, M.-L.; Hoof, S.; Braun-Cula, B.; Herwig, C.; Limberg, C. Switching from a Chromium(IV) Peroxide to a Chromium(III) Superoxide upon Coordination of a Donor in the Trans Position. *J. Am. Chem. Soc.* **2019**, *141*, 14068–14072.

(105) Ansari, A.; Jayapal, P.; Rajaraman, G. C-H Bond Activation by Metal-Superoxo Species: What Drives High Reactivity? *Angew. Chem., Int. Ed.* **2015**, *54*, 564–568.

(106) Hong, S.; Sutherlin, K. D.; Park, J.; Kwon, E.; Siegler, M. A.; Solomon, E. I.; Nam, W. Crystallographic and Spectroscopic Characterization and Reactivities of a Mononuclear Non-Haem Iron(III)-Superoxo Complex. *Nat. Commun.* **2014**, *5*, 5440–5446.

(107) Oddon, F.; Chiba, Y.; Nakazawa, J.; Ohta, T.; Ogura, T.; Hikichi, S. Characterization of Mononuclear Non-Heme Iron(III)-Superoxo Complex with a Five-Azole Ligand Set. *Angew. Chem., Int. Ed.* **2015**, *54*, 7336–7339.

(108) Chiang, C.-W.; Kleespies, S. T.; Stout, H. D.; Meier, K. K.; Li, P.-Y.; Bominaar, E. L.; Que, L.; Münck, E.; Lee, W.-Z. Characterization of a Paramagnetic Mononuclear Nonheme Iron-Superoxo Complex. *J. Am. Chem. Soc.* **2014**, *136*, 10846–10849.

(109) Kovacs and coworkers recently described a non-heme Fe^{III}-superoxide intermediate which abstracts hydrogen atoms from 1,4-cyclohexadiene (CHD) (BDE = 76 kcal/mol) but also THF solvent, that possessing a strong C–H bond (BDE = 92 kcal/ mol); an Fe^{III}-hydroperoxide complex is the product; Blakely, M. N.; Dedushko, M. A.; Poon, P. C. Y.; Villar-Acevedo, G.; Kovacs, J. A. Formation of a Reactive, Alkyl Thiolate-Ligated Fe^{III}-Superoxo Intermediate Derived from Dioxygen. *J. Am. Chem. Soc.* **2019**, *141*, 1867–1870.

(110) Curley, J. J.; Bergman, R. G.; Don Tilley, T. Preparation and Physical Properties of Early-Late Heterobimetallic Compounds Featuring Ir-M Bonds (M = Ti, Zr, Hf). *Dalt. Trans.* **2012**, *41*, 192–200.

(111) Mader, E. A.; Davidson, E. R.; Mayer, J. M. Large Ground-State Entropy Changes for Hydrogen Atom Transfer Reactions of Iron Complexes. *J. Am. Chem. Soc.* **2007**, *129*, 5153–5166.

(112) Wu, A.; Mader, E. A.; Datta, A.; Hrovat, D. A.; Borden, W. T.; Mayer, J. M. Nitroxyl Radical Plus Hydroxylamine Pseudo Self-Exchange Reactions: Tunneling in Hydrogen Atom Transfer. *J. Am. Chem. Soc.* **2009**, *131*, 11985–11997.

(113) Ghiladi, R. A.; Huang, H.-w.; Moënne-Loccoz, P.; Stasser, J.; Blackburn, N. J.; Woods, A. S.; Cotter, R. J.; Incarvito, C. D.; Rheingold, A. L.; Karlin, K. D. Heme-Copper/dioxygen Adduct Formation Relevant to Cytochrome *c* Oxidase: Spectroscopic Characterization of $[(^6L)Fe^{III}(O_2^{2-})Cu^{II}]^+$. *J. Biol. Inorg. Chem.* **2005**, *10*, 63–77.

(114) Wasser, I. M.; Huang, H.-w.; Moënne-Loccoz, P.; Karlin, K. D.

Heme/Non-Heme Diiron(II) Complexes and O_2 , CO , and NO Adducts as Reduced and Substrate-Bound Models for the Active Site of Bacterial Nitric Oxide Reductase. *J. Am. Chem. Soc.* **2005**, *127*, 3310–3320.

(115) Chufán, E. E.; Puiu, S. C.; Karlin, K. D. Heme-Copper/Dioxygen Adduct Formation, Properties, and Reactivity. *Acc. Chem. Res.* **2007**, *40*, 563–572.

(116) Kieber-Emmons, M. T.; Qayyum, M. F.; Li, Y.; Halime, Z.; Hodgson, K. O.; Hedman, B.; Karlin, K. D.; Solomon, E. I. Spectroscopic Elucidation of a New Heme/Copper Dioxygen Structure Type: Implications for O···O Bond Rupture in Cytochrome *c* Oxidase. *Angew. Chem., Int. Ed.* **2012**, *51*, 168–172.

Insert Table of Contents artwork here